Journal of Alloys and Compounds 1020 (2025) 179146

Contents lists available at ScienceDirect

Journal of Alloys and Compounds

journal homepage: www.elsevier.com/locate/jalcom

Review

# Development of a new ductile heat-treated multi-component aluminium by HPDC with high-performance properties for temperature applications

Ester Villanueva [a], Iban Vicario [a], Ignacio Crespo [a], Teresa Guraya [b], Iñaki Hurtado [c], Joseba Albizuri [b,*]

[a] Metal processing platform, TECNALIA, Basque Research and Technology Alliance (BRTA), Derio E48160, Spain
[b] Faculty of Engineering of Bilbao, University of the Basque Country (UPV/EHU), Bilbao E48013, Spain
[c] Mechanical and Manufacturing Department, Mondragon University, Arrasate-Mondragon E20500, Spain

ARTICLE INFO

*Keywords:*
Aluminium
Multicomponent
HPDC process
Thermal treatment
Properties
High temperature

ABSTRACT

This research aims to develop heat treatments to improve mechanical and thermal properties for a novel, heat-treatable patented multi-component AlMgSiCu aluminium produced using the High-Pressure Die Casting (HPDC) process. For this purpose, experiments were designed to investigate various parameters related to the thermal treatments, implemented in three stages. The alloy displayed excellent mechanical properties at room temperature (RT) and 200 ºC with an adjusted and optimized heat treatment: 440 °C solution treatment for 72 hours, hot-water quenching, and natural ageing. The alloy's microstructure consisted of an aluminium matrix with primary and eutectic $Mg_2Si$ and globular $Al_2CuMg$ phases, where all $Al_2Cu$ phases were transformed into $Al_2CuMg$. The thermal transformation of $Al_2Cu$ into the most stable $Al_2CuMg$ phase, significantly enhanced the alloy's overall properties, resulting in a 40 % increase in elongation (E) under tension with a yield strength (YS) of 221 MPa, an ultimate tensile strength (UTS) of 244 MPa, and an E of 1.1 %. Additionally, it led to a 20 % improvement in ultimate compressive strength (UCS), with a 60 % increase in compressive deformation (D) at RT compared with as-cast samples. At 200ºC the tensile properties remained stable, with a YS of 226 MPa, UTS of 254 MPa, and E of 1 %, while the UCS decreased by 30 % and both YS and D remained constant with a YS of 211 MPa, UCS of 468 MPa and a D of 25.1 %. Overall, the alloy demonstrated excellent performance, achieving some of the most favourable strength-to-density ratios at 200 ºC.

## 1. Introduction

Aluminium alloys, known for their lightweight properties, in combination with high degree of functionality, are highly attractive materials for the automotive industry. These alloys contribute to improved fuel efficiency [1], structural integrity, and overall performance of vehicles with a high recovery rate and are reused in new products [2]. Nowadays, the average total weight of a car in Europe is approximately 1500 kg [3], with aluminium accounting for 7–15 % [4], depending of the car model [5,6]. Currently, Mercedes-Benz and Stellantis are among the largest customers of aluminium, along with sports car manufacturers [7]. Reports predict that aluminium usage will increase by 15 % by 2026 compared to 2022, and by 24,9 % by 2030 [8].

For internal combustion engines, friction and weight reduction are important to contribute to fuel/energy economy. At the same time, a weight reduction can lead to the downsizing of engines and suspension systems, with an overall reduction in vehicle weight [9].

To ensure optimal performance, an elongated core made of ultra-high strength alloy is essential [10], providing both rigidity and resistance to deformation under high-stress conditions. Various works are striving to develop improved materials for automotive applications, but aluminium stands out as a particularly promising material due to its impressive strength-to-density ratio and thus utilized in numerous structural components [11]

At this point, it's noteworthy to highlight Tesla's pioneering role in introducing GIGAPRESS technology [12]. This production technology enables the injection and casting of large castings using special aluminium alloys with complex geometries and large dimensions [13]. Nowadays, approximately 50 % of the world's production of light metal castings is achieved through this technology, and the application of high-pressure aluminium die casting (HPDC) is expected to increase by 2040 [14].

* Corresponding author.
*E-mail address:* joseba.albizuri@ehu.eus (J. Albizuri).

https://doi.org/10.1016/j.jallcom.2025.179146
Received 25 November 2024; Received in revised form 4 February 2025; Accepted 10 February 2025
Available online 18 February 2025

Automotive alloys produced through the pressure die casting process are primarily based on the AlSiCu [15,16] and AlSiMg [17] systems, generally in the as-cast state. These alloys generally exhibit yield strength (YS) of 140 MPa and ultimate tensile strength (UTS) values of 240 MPa, with elongation (E) values of 1 % or less and hardness levels ranging between 70 and 80 HB [18]. Newly developed alloys, such as Silafon, which are based on AlSiMg(Mn), demonstrate improved elongation but exhibit lower yield strength values [19]. Although the primary unmodified phases of $Mg_2Si$ can provide high hardness, they are not good at reaching high ductility [20].

In addition, above 200ºC, both AlSiMg and AlSiCu alloys experience a significant reduction in strength, with YS decreasing by as much as 45 % and UTS dropping by over 50 % [21,22]. Additionally, hardness values decline by more than 20 % when temperatures reach 200 ºC [23].

Currently, new high-temperature aluminium alloys based on the AlSiCuMg system are under investigation [24,25], however, they display limited resistance under compressive loads.

In contrast, other alloys that are attracting significant interest are high entropy alloys or multicomponent alloys [26], which are notable for their substantial improvement in properties, particularly in compressive strength.

To meet the increasingly demanding requirements of automotive cast parts, which are subjected to higher pressures and temperatures, it is essential to enhance the performance of aluminium alloys. This can be also achieved through heat treatment or by adjusting the chemical composition [27].

Thermal treatments are effective for enhancing the microstructure and therefore the mechanical properties resulting in higher strength, increased hardness, and improved elongation [28]. However, aluminium casting alloys produced by HPDC can exhibit some defects that restrict their heat-treatability, making it difficult to improve their mechanical properties [29].

The trend in the development of structural HPDC aluminium alloys is focused on non-heat treatable options [30]. In some works, new more favorable heat treatable casting alloys, such as AlMgSi(MnZr) alloy are currently under development [31].

Among the various thermal processes for die-casting aluminium alloys, the T5, T6, and T7 heat treatments are the most widely applied, with T6 offering the highest resistance [32]. T6 is completed in three steps: solubilization; tempering and ageing. During the solution treatment, the alloy is heated to a temperature just below its initial melting point. It is maintained at this temperature long enough to dissolve the maximum possible number of alloying elements into the matrix, achieving a high and uniform concentration of these elements in a solid solution. During this process three primary purposes are served: homogenization of as-cast structure, dissolution of certain intermetallic phases such as $Al_2Cu$ or $Mg_2Si$ and change of the morphology of eutectic silicon from the fragmentation to spheroidization [33]. Then, the alloy is rapidly cooled to obtain a supersaturated solid solution of solute atoms and vacancies, thereby inhibiting the precipitation of coarse grain boundary precipitates [34]. For tempering, different processes can be used, cold water is generally the most employed [35]. Finally, during the ageing process, the alloy is heated to a specific temperature, causing the precipitation of solute atoms from the supersaturated solid solution [36].

The precipitation sequence in aged AlSiMg alloys is from supersaturated solute solution (SSS) → (Si and Mg clusters) → Mg+Si co-clusters → Guinier-Preston (GP) zones → Intermediate phase ($\beta''$) →Intermetallic phase ($\beta'$) →Equilibrium phase ($\beta$) [37]. In the AlSiMgCu alloy the process is similar, but more complex phases as the Q''($Al_5Mg_8Si_6Cu_2$) and the θ'($Al_2Cu$) phase may also be formed [38].

In addition to the type of chemical composition of the alloy, several factors, including temperature, holding time, and cooling rate, will affect its mechanical and physical properties. ASTM B917 and ASTM B91 set the process parameters, but they may not be optimal for all applications [39].

The effect in hardness value by applying heat treatments at different solution temperatures (520 ºC, 530 ºC, and 540 ºC) and times (from 2 to 5 hours), has been investigated in AlSi base alloys. The maximum hardness values were achieved at the temperature of 540 ºC, quenching in water at RT, and ageing process at 180 ºC for 3 h [40]. As a result, the microstructure was characterized by the dissolution of $Mg_2Si$ into the aluminium matrix and the globulization of Si particles. Regarding iron intermetallics, AlFeSi remained stable, but the AlSiMgFe phase was completely converted into the detrimental beta AlFeSi [41]. Thus, the duration of the thermal process was crucial.

In other studies, the prolonged holding solution time after 60 minutes was found not to affect the tensile properties of AlSi(Mg) casting alloys [42]. In aluminium HPDC alloys, it has been demonstrated that defects such as blistering can be prevented by employing significantly shorter solution treatment times and lower temperatures [43]. However, aluminium alloys containing Cu can need a time of 40 hours or more to facilitate complete homogenization [44,45]. In the AlSi(MgMn) HPDC alloy, raising the solution temperature from 475 °C to 525 °C enhanced the mechanical properties without causing blistering issues. YS increased by 70 % and continued to rise with longer solution times. Conversely, the UTS was unaffected by time, while E showed only a slight increase [46]. In other studies focusing on AlSi(MgCu) alloys, a duration of 4 hours at 490 °C was found to be sufficient for achieving complete dissolution and homogenization of intermetallics. However, if magnesium is not added, the process may require up to 8 hours [47].

Relating to the ageing process, a series of ageing temperature and time values between 155 and 170 ºC and from 3.5 h to 6.5 h were varied on AlSi(Mg) alloys while the solution treatment was kept constant [48]. The maximum values of the quality index [49], UTS and E were achieved at the temperature of 155 °C for a duration of 5.5 hours. Contrastingly, in one case of AlSi(MgCu) alloy, the peak hardness was attained at 175 °C after 1 hour [50], while in other cases, over-aged structures in AlSi(MgCu) alloy did not manifest until after ageing for 100 hours at 160 °C [51]. The $Mg_2Si$ is an important strengthening phase in the aluminium alloys. The higher the quantity of Mg and the ageing temperature, the greater the YS and UTS [52]. However, while artificial ageing of AlSi(Mg) alloys in the temperature range of 170–210 °C can lead to the attainment of comparable peak yield strengths, Cu-containing alloys can exhibit a decrease in YS as the ageing temperature increases [47,53].

In other studies, additional parameters such as water quenching at high temperatures (75–90 ºC) were also investigated to enhance the mechanical properties [54,55].

The effect of a two-step multi-stage solution treatment is being proposed [56,57]. In the case of AlSi(Cu) alloy, the sample submitted to two solution processes, heated at 485 ºC and 515 ºC, presented better mechanical properties in terms of hardness, UTS, and E [58]. For AlSi(CuMg) alloy, the higher value for hardness was obtained by applying artificial ageing for 6 h at 180 °C after the double-stage solution treatment and quenching. The first solution process was carried out at 495 ºC for 6 hours to dissolve the low melting compounds and the second solution process at a higher temperature of 515 ºC for 2 hours [59]. Otherwise other studies for AlSi(Mg) alloys confirmed there's no convincing justification for utilizing a two-step or multistage solution treatment [60].

The use of models facilitates the design of a heat treatment process. The dissolution and formation of phases can be well predicted by the equilibrium phase diagrams obtained by the software FactSage, ThermoCalc, or Pandat [61]. Differential scanning calorimetry (DSC) [62] or Thermal Analysis (TA) [63] can be employed to determine the most adequate solution temperature. Also, TA techniques based on the study of cooling curves, are a widely used quality control system in aluminium casting plants [64]. This technique is highly effective for determining the parameters characteristic of the solidification process, including the precipitation phases of the different intermetallics; therefore, it can be applied in the design of thermal treatments [65,66]. A cooling curve represents the balance between heat evolution in the sample and the

dissipation. Its shape, measured by a thermocouple, indicates the solidification process, which is influenced by factors like chemical composition, modifiers, etc. The cooling curve's shape correlates with the composition, microstructure, and mechanical properties under a fixed production condition [67]. Without phase transformations, the curve shows a constant negative slope, dictated by heat transport, mass, and heat capacity. During phase transformations, the slope shifts positively, influenced by the latent heat and fraction of the material transformed [68].

This research focuses on developing a new heat-treatable multicomponent aluminium alloy with enhanced mechanical properties at RT and 200 ºC. The alloy is based on the Al80Mg10Si5Cu5 system and was produced using the HPDC foundry process. Experiments have been designed to investigate various parameters to identify the optimal thermal treatment. FactSage and TA techniques were employed for adjusting the thermal treatment temperatures and times. Simulation data were compared with the experimental results. Finally, once the optimal thermal treatment was selected, the physical and mechanical properties at both RT and 200 ºC were evaluated for comparison.

## 2. Materials and methods

### 2.1. Materials and samples preparation

The casting of the Al80Mg10Si5Cu5 alloy was carried out using the HPDC casting process at the Tecnalia pilot foundry, as depicted in Fig. 1. In each cycle or shot, two standard-sized tensile bars were produced. In total, 100 cycles were completed, resulting in the production of 200 standard tensile bars. The cycle time was 57 seconds and an in-mould pressure of 800 bar. The temperature of the alloy before the pouring process was set to 700 ºC, while the mould temperature was maintained at 300 ºC. The speed of the first plunger was set to 0.4 m/s, while the second plunger was set to 3.2 m/s.

The chemical composition of the obtained Al80Mg10Si5Cu5 alloy, measured with an Optical Emission Spectrometer (OES), is displayed in Table 1. The main alloying elements of the new multicomponent aluminium alloy were magnesium (Mg), silicon (Si), and copper (Cu).

The microstructure of the Al80Mg10Si5Cu5 alloy in the as-cast condition is shown in Fig. 2. The microstructure comprised of an aluminium-rich matrix reinforced with primary and eutectic $Mg_2Si$ particles, along with interdendritic phases of $Al_2Cu$ and $Al_2CuMg$. Particle sizes were measured from SEM images using ImageJ software. The primary $Mg_2Si$ particles varied in size from 9 to 32 μm, with an average of 21 ± 7.97 μm, while the eutectic $Mg_2Si$ particles measured 4.2 ± 1.46 μm. The $Mg_2Si$ particles exhibited various shapes and distributions, which can result in the emergence of stress compatibilities between the matrix and these brittle phases and therefore cause premature failure [69]. The phases of $Al_2Cu$ and $Al_2CuMg$ solidified within the interdendritic region. The average aluminium grain size was about 5,66 ± 1,75 μm.

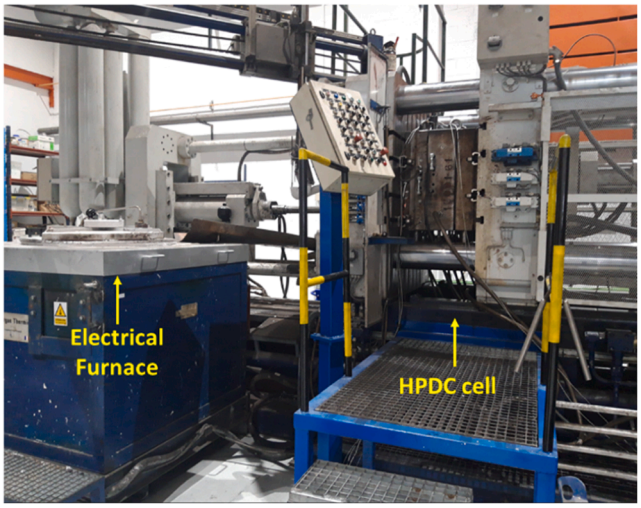


**Fig. 1.** Detail of HPDC machines.

**Table 1**
Chemical composition (wt%) of the Al80Mg10Si5Cu5 multicomponent aluminium alloy by OES.

| Method | Al | Mg | Si | Cu | Fe | Mn |
|---|---|---|---|---|---|---|
| OES | 79.3 | 9.2 | 4.7 | 6.1 | 0.4 | 0.3 |

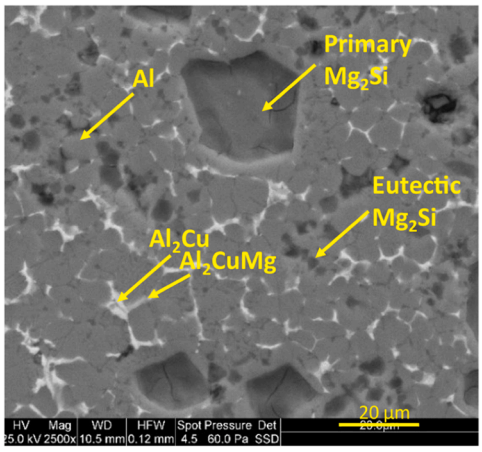


**Fig. 2.** SEM microstructure of the as-cast Al80Mg10Si5Cu5 alloy.

The mechanical and physical properties at RT were evaluated. The hardness value was 156 ± 6.7 HV3. Tensile properties exhibited a YS of 311 ± 5,7 MPa, a UTS of 316 ± 2.08 MPa, and an elongation of 0.6 ± 0.1 %. The reduced ductility was attributed to stress incompatibilities at the interfaces between unmodified brittle particles, which remain under elastic strain, and a matrix undergoing plastic deformation [20], leading to premature particle cracking [70]. The compressive strength (UCS) reached 646 ± 8.08 MPa, with a YS of 362 ± 6.0 MPa and a deformation (D) of 12 ± 1.15 %. In addition, the alloy's electrical conductivity was 18 ± 0.29 % IACS, and its density was 2.59 g/cm$^3$.

### 2.2. Phase simulation by FactSage

To investigate the different precipitated phases and their solidification temperatures, FactSage version 8.3 and database FTlite software were applied by inputting the real chemical composition. FactSage is one of the largest fully integrated database computing systems in chemical thermodynamics based on the CALPHAD Methodology (Computer Coupling of Phase Diagrams and Thermochemistry, originally known as CALculation of PHAse Diagrams).

The equilibrium (Fig. 3) and non-equilibrium - Scheil diagrams (Fig. 4) are shown below. According to the figures, under equilibrium, liquidus ranged between 623 ºC and 511 ºC; while under non-equilibrium conditions, solidification occurred later, at the temperature of 503 ºC.

Simulation under equilibrium conditions predicted the solidification of a significant amount (around 80 %) of FCC aluminium solid solution at 594 ºC. The $Mg_2Si$ phase precipitated before aluminium nucleation at 623 ºC, forming primary $Mg_2Si$ particles, and continued precipitating alongside the aluminium during the solidification process. T-$Al_2Cu$ began to precipitate at 511 ºC, later some of this transforming into the S-phase ($Al_2CuMg$) phase at 441 ºC. Additionally, $Al_7CuMn_2$ and

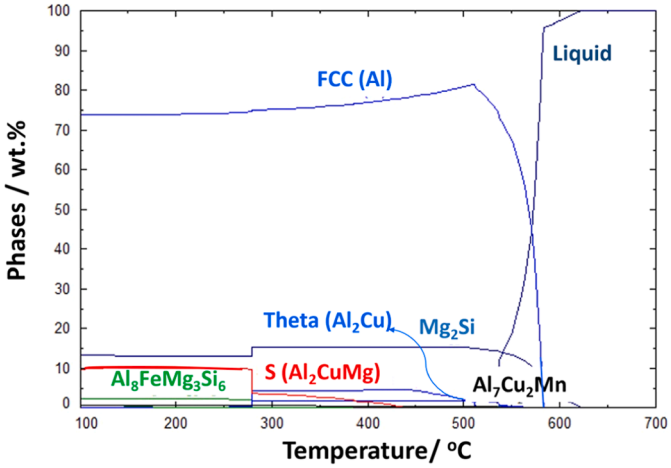


**Fig. 3.** Equilibrium solidification (simulation) of Al80Mg10Si5Cu5 alloy.

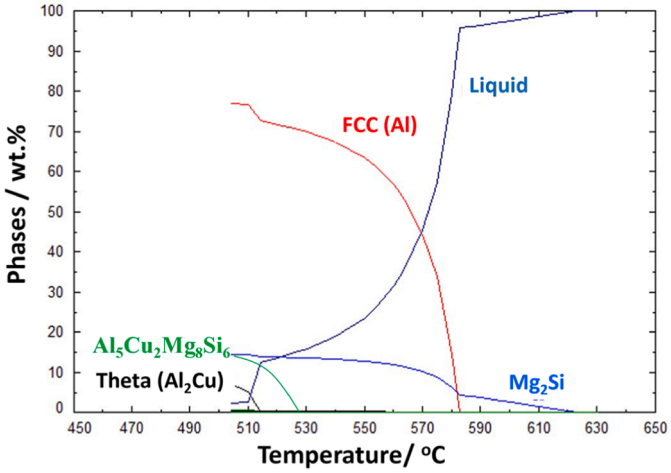


**Fig. 4.** *Scheil* solidification (simulation) of Al80Mg10Si5Cu5 alloy.

$Al_8FeMg_3Si_6$ phases appeared.

Under non-equilibrium conditions, primary $Mg_2Si$ was precipitated at 623 ºC, with the FCC aluminium precipitating at 583 ºC, followed by T-phase-$Al_2Cu$ at 514 ºC along with minor $Al_7CuMn_2$, $Al_8FeMg_3Si_6$, and AlFeSi (minor than 0.5 %). Instead, the $Al_5Cu_2Mg_8Si_6$ was predicted with a percentage of less than 0.5 %.

### 2.3. Application of thermal analysis (TA)

Cooling curves were determined by setting type K thermocouples in the center of metal moulds and pouring the molten metal preheated to approximately 100 °C (720 °C in our case) above its liquidus temperature. The masses obtained weighted approximately 300 ± 10 g. Temperatures between 630–400 °C were recorded. The data of the TA were collected using a high-speed National Instruments Data Acquisition System linked to a personal computer collecting temperature data every 10 data per second. Each TA trial was repeated three times. Finally, cooling curves are obtained by plotting the measured temperatures at equal-time intervals. Afterward, smoothing was applied to both the cooling curve and the derivatives using the moving average method using Python software version 3.12 (2023).

The studied cooling curves and their derivatives are shown in Fig. 5. The CALPHAD simulation results were initially used to estimate the precipitating phases. They were validated through XRD, OM, and SEM+EDS analysis. The determined phases in the TA curve had been

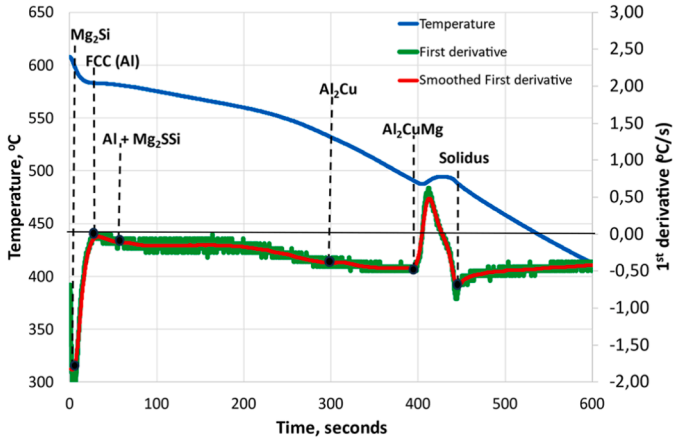


**Fig. 5.** Cooling-curve and 1st derivative curves of Al80Mg10Si5Cu5 alloy (experimental results).

correlated with CALPHAD, XRD, OM, and SEM+EDS defined phases.

The TA curve presented the precipitation of 5 different phases. Primary $Mg_2Si$ nucleated at 592 ºC. The aluminium phase precipitated and grew between 582 and 579.9 ºC. The eutectic $Mg_2Si$ solidification started at 574.8 ºC and continued until 570.7 ºC. $Al_2Cu$ precipitated at 529 ºC, reaching its maximum growth at 511 ºC. The intermetallic $Al_2CuMg$, with a lower melting point [71], nucleated at 487.6 ºC with a recalescence observed at 491.8 ºC [72]. Finally, the solidus temperature was reached at 482.2 ºC.

### 2.4. Design parameters

In the present study, the effects and development of thermal treatments were analyzed in three levels.

In the first level, as shown in Table 2, the design parameters included a range of solution and precipitation treatment temperatures. Given that the approximate solidification temperatures were 503–511 ºC by FactSage but 482.2 ºC based on TA, it was decided to set lower solid solution temperatures to avoid melting of non-equilibrium phases. The defined temperatures were as follows: 380 ºC (Condition 1), 410 ºC (Condition 2) and 440 ºC (Condition 3). For comparison, a higher temperature of 460 ºC (Condition 4) was also selected. Regarding the ageing temperature three different values were selected: for each condition: 160, 190, and 220 ºC. For the highest solution temperature (condition 4), the selected range of ageing temperatures was slightly higher. To reduce the number of tests, it was proposed to perform the tests with fixed times for both the solution and ageing treatments. Additionally, a common quenching process in water at 25 °C was established.

In the second level, new casting parts were produced. Also in the second level, as detailed in Table 3 and by following the selection of the two most effective thermal treatments, additional parameters were adjusted. The decision was made to extend the holding time for solution treatments from 24 to 72 hours to ensure a complete dissolution of precipitates. Additionally, the cooling process was optimized by quenching in water at 75 °C to mitigate residual stresses observed in certain casting components [55,73].

Finally, after adjusting the various parameters of heat treatment, including the solution time and quenching temperature, the optimal heat-treatment process was successfully reproduced, allowing for more detailed analyses to be carried out. The final selected treatment was #3a: solution temperature of 440 ºC for 72 h, quenching in water at 75 ºC, followed by natural ageing.

### 2.5. Development of thermal treatment process

The thermal treatment process was conducted using a Nabertherm

**Table 2**
Heat treatments design in level 1.

| Condition | Ref. | Solution (ºC) | Ageing (ºC) | Hold time Solution (h) | Cooling Solution | Hold time Ageing (h) | Cooling Ageing |
|---|---|---|---|---|---|---|---|
| #1 | #1a | 380 | - | 24 | Water at 25 ºC | 4 | Air |
| | #1b | | 160 | | | | |
| | #1c | | 190 | | | | |
| | #1d | | 220 | | | | |
| #2 | #2a | 410 | - | | | | |
| | #2b | | 160 | | | | |
| | #2c | | 190 | | | | |
| | #2d | | 220 | | | | |
| #3 | #3a | 440 | - | | | | |
| | #3b | | 160 | | | | |
| | #3c | | 190 | | | | |
| | #3d | | 220 | | | | |
| #4 | #4a | 460 | - | | | | |
| | #4b | | 200 | | | | |
| | #4c | | 220 | | | | |
| | #4d | | 240 | | | | |

**Table 3**
Heat treatment design in level 2.

| Condition | Ref. | Solution (ºC) | Ageing (ºC) | Hold time Solution (h) | Cooling Solution | Hold time Ageing (h) | Cooling Ageing |
|---|---|---|---|---|---|---|---|
| #3 | #3a´ | 440 | - | 72 | Water at 75 ºC | 4 | Air |
| | #3b´ | | 160 | | | | |

LH 60/13 model chamber furnace. To ensure precise temperature control, a thermocouple type K was inserted and monitored throughout the process. The thermal treatments were applied to the tensile standard bars in their as-cast condition.

In each test condition of level 1 and level 2, the microstructure was analyzed using an optical microscope (OM) and scanning electrical microscopy (SEM). Additionally, the mechanical properties (hardness and tensile properties), and physical properties such as electrical conductivity were analyzed.

Once the best thermal treatment was validated in level 3, further analysis was conducted at both RT and 200 ºC. The comprehensive study of the microstructure included not only OM and SEM+EDS but also X-ray diffraction (XRD) tests.

### 2.6. Analysis of microstructure

#### 2.6.1. OM and SEM

The microstructures of the heat-treated (HT) samples were examined using an OM Leica DMI5000M (LEICA, Wetzlar, Germany) and a SEM EI Quanta 450 (FEI, Hillsboro, OR, USA) equipped with EDX analysis. Samples for metallographic evaluation were prepared following standard metallographic procedures. To ensure representative results, all the samples were extracted transversely from the neck of the tensile specimens.

#### 2.6.2. XRD

XRD patterns and mineralogical information were acquired utilizing a Philips X'Pert Pro MPD PW3040/60 X-ray diffractometer (Malvern Panalytical Ltd, United Kingdom) equipped with a copper anode running at a voltage of 40 kV and 40 mA (1.6 kW). Scans were executed over a 2θ range from 10° to

90°, with a step size of 0.02° 2θ, and each scan lasted 2 seconds. The X-ray diffraction patterns were matched against the PDF-2 database from the International Center for Diffraction Data (ICDD). XRD experiments were conducted on HT-samples at both RT and 200 ºC.

### 2.7. Analysis of mechanical properties

#### 2.7.1. Hardness

The hardness at RT of the HT- samples was analyzed using the Vickers test according to ISO 6507–1. The Vickers hardness was determined utilizing a Vickers hardness tester model FV-700, applying a load of 3 kgf.

Once the best thermal treatment was selected, tests at higher temperatures (200 ºC, 250 ºC and 300 ºC) were conducted. In this case, the tests were performed using a 713SRDM Rockwell (HOYTOM) equipment with a 100 kgf load and a 2.5 mm diameter ball indenter. For the heating process, the samples were heated and maintained at the testing temperature for around 50 minutes. A heating chamber Instron model 3119–406 was used. The obtained measurements were then converted into Vickers hardness numbers to compare with the hardness data at room temperature. It's important to note that these high-temperature tests are non-standardized.

To ensure representative results, ten measurements were taken from each sample from the surface layer to the interior.

#### 2.7.2. Tensile strength

The HT-samples underwent tensile strength testing at RT following UNE EN ISO 6892–1 using an Instron 5500R6025 device with a load range from 1 to 100 kN.

For high-temperature tests, once the best thermal treatment was validated, tests were conducted following UNE EN ISO 6892–2 at the temperature of 200 ºC. For this purpose, a heating chamber (Instrom 3119–007) was used to facilitate the heating process.

In each tensile test, three samples were employed to obtain accurate values with their variability.

#### 2.7.3. Compressive strength

The compression tests at RT and 200 ºC were performed using the same equipment as the tensile tests, following ASTM E-9 standard. Cylindrical specimens, 12 mm in diameter and 20 mm in length were extracted and machined from the head section of the tensile test specimens. At least three specimens were used for each test evaluation.

### 2.8. Analysis of physical properties

#### 2.8.1. Electric conductivity

The influence of heat treatments applied to the samples on electric conductivity was evaluated using a portable Autosigma 3000 model conductivity meter which reports the values in the standard unit %IACS (International Annealed Copper Standard).

## 3. Results and discussion

### 3.1. Results level 1

#### 3.1.1. Microstructure of HT-samples

Fig. 7-Fig. 10 show the micrographs of HT-samples.

In condition #1 in Fig. 6, with a solid solution treatment at 380 ºC and under the different ageing temperatures (from #1b to #1d), the $Mg_2Si$ particles did not exhibit proper solubilization. Some primary $Mg_2Si$ particles exceed 20 μm and maintained sharp, unmodified edges. Additionally, the microstructure revealed undissolved, agglomerated, and non-homogeneous eutectic $Mg_2Si$ structures [74].

In condition #2 in Fig. 7, with a solid solution treatment at 410 ºC, the sharp edges on primary $Mg_2Si$ particles were reduced, and the eutectic $Mg_2Si$ particles were fragmented into smaller, more spheroidized forms within the matrix [74]. As the ageing treatment temperature increased (from #2b to #2d), the number of globular eutectic $Mg_2Si$ particles increased, leading to more uniform dispersion. However, some agglomerated phases remained present.

In condition #3 in Fig. 8, with the solid solution temperature of 440 ºC, the size of primary $Mg_2Si$ particles was like Condition #2. A further reduction in sharp edges was observed, and more globular eutectic $Mg_2Si$ phases appeared within the matrix. This resulted in fewer agglomerated structures, a more uniform distribution, and a higher volume of precipitates.

Finally, in condition #4 in Fig. 9, samples subjected to a solid solution temperature of 460 ºC were analyzed. Comparison between conditions #3 and #4 revealed that samples subjected to condition #4 exhibited coarser $Mg_2Si$ particles, exceeding 24 μm and larger Cu-rich phases around 10 μm, compared to 21 μm and 5.4 μm, respectively, in condition #3. This suggests that over-modification occurred [75].

In conclusion, it was observed that the higher the solution temperature, the lower the number and size of $Mg_2Si$ particles and $Al_2Cu$ particles. For the same solution temperature, it was found that the higher the ageing temperature, the smaller the particle size, although at condition #c (190 °C), larger particles began to thicken, leading to the

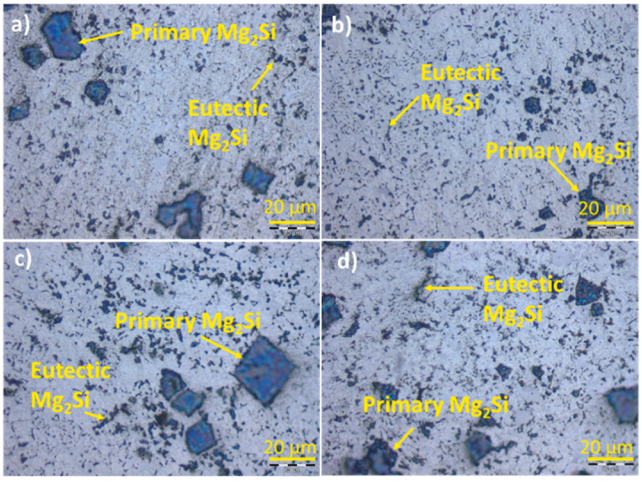


**Fig. 6.** x1000 MO of the HT-samples under condition #1 level 1: a) #1a (380 ºC), b) #1b (160 ºC), c) #1c (190 ºC), d) #1d (220 ºC).

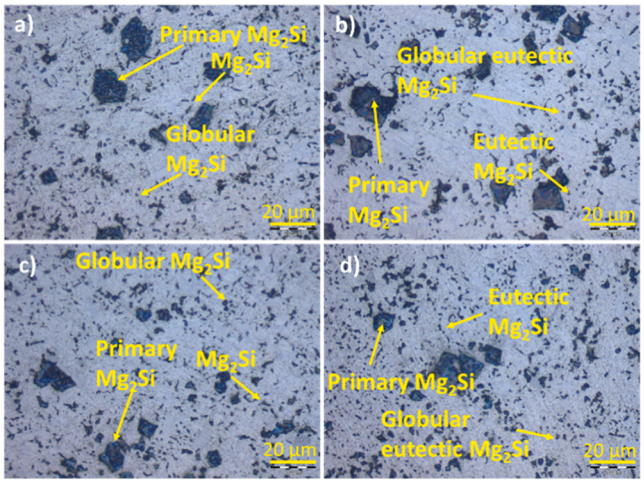


**Fig. 7.** x1000 MO of the HT-samples under condition #2 level 1: a) #2a (440 ºC), b) #2b (160 ºC), c) #2c (190 ºC), d) #2d (220 ºC).

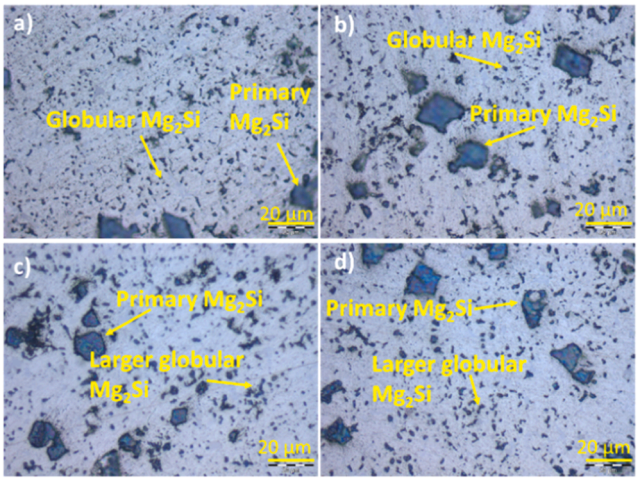


**Fig. 8.** x1000 MO of the HT-samples under condition #3 level 1: a) #3a (440 ºC), b) #3b (160 ºC), c) #3c (190 ºC), d) #3d (220 ºC).

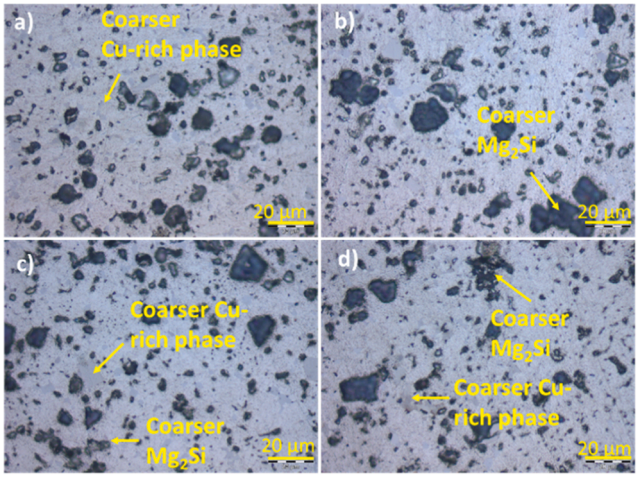


**Fig. 9.** x1000 MO of the HT-samples under condition #4 level 1 (480 ºC), b) #4b (200 ºC), c) #4c (220 ºC), d) #4d (240 ºC).

coarsening of the particles.

After completing the analysis of samples, it was concluded that the best structures were achieved under condition #3 (solid solution temperature of 440 ºC). Case #3a (without ageing treatment) and #3b (with ageing treatment at the temperature of 160 ºC) were identified as the most promising options.

Table 4, Table 5, and Table 6 summarize the values for the percentage of area of each phase, average size and shape factor.

By applying a solubilization treatment, the FCC aluminium matrix percentage increases compared with the as-cast state. As we increase the percentage of dissolved alloyed elements in the matrix, the percentage of aluminium area increases.

As we increase the solubilization temperature, the average FCC aluminium matrix area is increased, showing a higher dissolution of alloying elements and phases into the matrix. In parallel, both primary and eutectic $Mg_2Si$ reduce their average area percentage of the area by increasing the solubilization temperature. In the case of Cu-phases, there is not a clear tendency, to maintain near-stable percentages by variating the solubilization temperatures, probably by the smaller precipitation temperatures (about 280 ºC in FactSage equilibrium simulation) of a majority percentage of the $Al_2CuMg$ phase.

The ageing temperatures showed in general, that optimal ageing temperatures are obtained in the middle of the selected ageing temperatures.

In general, the grain size of aluminium was increased by applying a solubilization treatment. This can be correlated with the dissolution of alloying elements into the FCC Al matrix and the reduction of other phases in the microstructure. The ageing treatment promoted the precipitation of solubilized alloying elements, decreasing the Al grain size at intermediate ageing temperatures. This can be related with the sub or over modification of precipitating phases.

In $Mg_2Si$ primary samples particle area, it can be observed that the higher the solubilization temperature promoted a decrease in the average area, linked with a partial dissolution of primary $Mg_2Si$ particles in the FCC Al matrix. It's well known that the higher the solution temperature and residence time, the higher the $Mg_2Si$ dissolution in the aluminium matrix. The higher ageing temperature promotes an over ageing of the alloy, promoting the coarsening of the $Mg_2Si$ particles and increasing its size. A similar tendency is observed with the eutectic $Mg_2Si$.

Cu particle area decreased slightly with the solubilization treatment but only at the highest solubilization temperature. The higher ageing temperatures promoted an over ageing of the alloy, promoting the coarsening of the Cu particles and increasing its area.

The S.F. is related to the sphericity of phases. A value of 1 would be correlated with a perfect circle. The thermal treatments resulted in an increased S.F. value of the eutectic $Mg_2Si$ and Cu phases, indicating a spheroidization of them. An increase in the solution treatment temperature resulted in a higher shape factor in the intermediate temperature, indicating coarsening and agglomeration at high ageing temperatures.

**Table 4**
Phase Percentage in area of the different elements in level 1.

| Ref. | % Al | % $Mg_2Si$ primary | % $Mg_2Si$ eutectic | % Cu-phases |
|---|---|---|---|---|
| **As-Cast** | 78.8 | 7.3 | 5.3 | 8.6 |
| **#1a** | 78.7 | 9.2 | 5.7 | 6.4 |
| **#1b** | 82.9 | 4.9 | 6.0 | 6.2 |
| **#1c** | 79.8 | 2.1 | 10.0 | 8.1 |
| **#1d** | 82.4 | 6.8 | 4.7 | 6.1 |
| **#2a** | 78.9 | 5.0 | 6.4 | 9.6 |
| **#2b** | 82.1 | 6.9 | 4.4 | 6.6 |
| **#2c** | 82.1 | 6.4 | 7.0 | 4.4 |
| **#2d** | 80.9 | 4.7 | 8.9 | 5.5 |
| **#3a** | 85.3 | 4.7 | 6.3 | 3.8 |
| **#3b** | 83.8 | 4.4 | 6.8 | 5.1 |
| **#3c** | 83.3 | 3.4 | 6.7 | 6.6 |
| **#3d** | 78.7 | 5.8 | 7.7 | 7.8 |
| **#4a** | N/A | 11.3 | 6.5 | N/A |
| **#4b** | N/A | 13.0 | 8.9 | N/A |
| **#4c** | N/A | 11.8 | 7.0 | N/A |
| **#4d** | N/A | 10.0 | 5.8 | N/A |

*N/A: Not Available.

**Table 5**
Average size and area of the different elements in level 1.

| Ref. | Grain size Al (μm) | Area Mg primary ($μm^2$) | Area Mg eutectic ($μm^2$) | Area Cu ($μm^2$) |
|---|---|---|---|---|
| **As-Cast** | 5.7 | 41.6 | 2.7 | 4.6 |
| **#1a** | 8.0 | 83.3 | 2.6 | 4.3 |
| **#1b** | 5.0 | 54.2 | 1.7 | 4.5 |
| **#1c** | 7.0 | 162.7 | 2.3 | 9.4 |
| **#1d** | 6.4 | 156.8 | 2.9 | 3.2 |
| **#2a** | 7.6 | 182.0 | 2.1 | 7.3 |
| **#2b** | 6.3 | 95.0 | 3.2 | 3.4 |
| **#2c** | 6.5 | 99.4 | 3.0 | 4.1 |
| **#2d** | 7.7 | 81.3 | 3.6 | 7.0 |
| **#3a** | 8.8 | 116.2 | 3.0 | 5.0 |
| **#3b** | 7.1 | 55.6 | 3.6 | 3.4 |
| **#3c** | 8.2 | 44.9 | 3.3 | 4.0 |
| **#3d** | 8.0 | 124.8 | 2.7 | 6.9 |
| **#4a** | N/A | 73.1 | 4.9 | N/A |
| **#4b** | N/A | 116.4 | 5.7 | N/A |
| **#4c** | N/A | 70.4 | 4.9 | N/A |
| **#4d** | N/A | 103.5 | 1.7 | N/A |

*N/A: Not Available.

**Table 6**
**Shape factor (S.F.)** of the different elements in level 1.

| Ref. | S.F. Mg primary | S.F. Mg eutectic | S.F. Cu |
|---|---|---|---|
| **As-Cast** | 0.20 | 0.30 | 0.38 |
| **#1a** | 0.36 | 0.47 | 0.45 |
| **#1b** | 0.11 | 0.28 | 0.41 |
| **#1c** | 0.16 | 0.49 | 0.37 |
| **#1d** | 0.37 | 0.49 | 0.48 |
| **#2a** | 0.34 | 0.53 | 0.50 |
| **#2b** | 0.34 | 0.52 | 0.55 |
| **#2c** | 0.27 | 0.51 | 0.77 |
| **#2d** | 0.30 | 0.46 | 0.49 |
| **#3a** | 0.20 | 0.37 | 0.43 |
| **#3b** | 0.27 | 0.55 | 0.60 |
| **#3c** | 0.36 | 0.58 | 0.61 |
| **#3d** | 0.35 | 0.57 | 0.52 |
| **#4a** | 0.38 | 0.60 | N/A |
| **#4b** | 0.30 | 0.57 | N/A |
| **#4c** | 0.39 | 0.58 | N/A |
| **#4d** | 0.29 | 0.69 | N/A |

*N/A: Not Available.

### 3.1.2. *Mechanical properties of the HT-samples*

*3.1.2.1. Hardness.* Fig. 10 presents the hardness values of HT-alloys from condition #1 to condition #4.

Condition #3 (3a, 3b, 3c) and #4b achieved the highest hardness levels, around 140 HV3, with a reduction of no more than 10 % compared to the as-cast sample.

In contrast, condition #1 showed the lowest hardness values, reaching a maximum of 109 HV3, representing an approximate 21 % reduction relative to the as-cast samples.

It is worth noting that the hardness of the HT-Al80Mg10Si5Cu5 alloy in all cases was generally lower than that of the as-cast alloy. This may be due to softening by grain growth [76] and the fragmentation of the high-hardness intermetallic compounds present in the as-cast Al80Mg10Si5Cu5 alloy [77].

Condition #1 (solution temperature of 380 ºC) presented the lowest hardness values among the samples. The lower hardness values can be

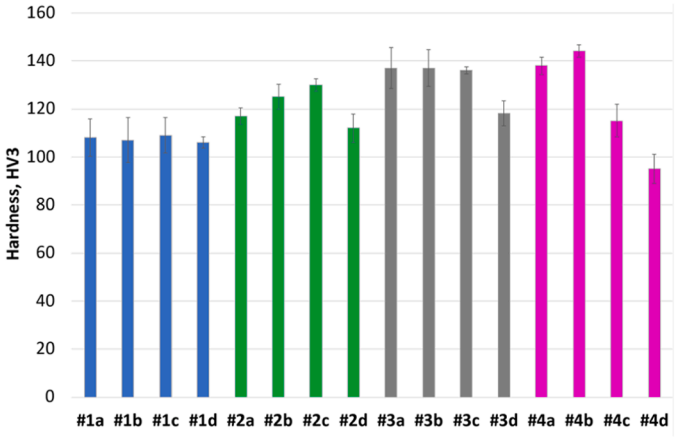


**Fig. 10.** Hardness values HT-Al80Mg10Si5Cu5 from condition #1 to #4 (experimental results).

attributed to the presence of unmodified primary $Mg_2Si$ particles and non-homogeneous precipitation of eutectic $Mg_2Si$, as observed in the microstructure. Under condition #1, the various ageing temperatures (#1b-#1d) did not significantly impact the hardness results, with values remaining very similar to those obtained without additional ageing treatment (#1a).

Under condition #2 (solution temperature of 410 ºC), hardness values were higher compared to the previous case, although they remained significantly lower than those observed in as-cast condition. This increase can be attributed to the improved morphology of $Mg_2Si$ particles. However, from the ageing temperature of 190 °C (case #2c), a sharp decline in hardness values was observed, mainly due to the gradual coarsening of some eutectic $Mg_2Si$ particles [78].

Under condition #3 (solution temperature of 440 ºC), the hardness values increased significantly, reaching values comparable to those observed in the as-cast state. This improvement is attributed to the more regular morphology of primary $Mg_2Si$ particles and the spheroidized, homogeneously dispersed eutectic $Mg_2Si$ particles throughout the matrix, resulting from better precipitate dissolution. In cases #1a, #1b and #1c, the properties remained constant as the ageing temperature increased. However, starting from the ageing temperature of 190 ºC (case #3c), hardness decreased by about 10 %. This reduction is likely due to the gradual coarsening of some eutectic $Mg_2Si$ particles or the precipitation of additional intermetallic phases at the grain boundaries, which cause segregation and further coarsening [79–81].

Finally, under condition #4 (solution temperature of 460 ºC), the hardness values were very similar to those of case #3. However, after ageing at 220 ºC, the hardness values dropped by nearly 20 %. This reduction is likely due to the increased presence of coarser Mg and Cu-rich phases in the microstructure [78].

It was confirmed that the higher the solid solution temperature, the higher the hardness values obtained [82], which is related to precipitation of finely and uniformly coherent $Mg_2Si$ precipitates [83].

Additionally, it was observed that higher ageing temperatures initially increased hardness, but when treatments exceeded 190 °C, the hardness values decreased again. This decrease is likely due to the transformation of precipitates from coherent to semi-coherent, and the coarsening of eutectic intermetallics [84]. When the alloy was solution treated under the most severe conditions (460 ºC), over-saturation occurred, increasing the hardness initially. However, subsequent ageing caused a significant reduction in hardness. This decrease in hardness is attributed to the excessive coarsening and coalescence of the precipitated phases [85].

It was found that the optimum heat treatment to achieve maximum hardness was under condition #3, with a solution temperature of 440 °C. A comparison of conditions #3a, #3b, and #3c indicated that with ageing up to a temperature of 190 °C, the values remained stable.

It was demonstrated that the values achieved in all conditions significantly surpassed those of commercial alloys according to the UNE EN-1706 standard, which typically ranges between 60 and 85 HV [21]. Given that the obtained values were higher, it is anticipated that the temperature properties in the final phase will exceed those of the alloys currently in use.

### 3.2. *Tensile strength*

The tensile engineering properties, Yield Strength (YS), Ultimate tensile Strength (UTS), and Elongation (E), obtained in each heat treatment condition are collected in Fig. 11-Fig. 13.

Regarding YS, condition #1 exhibited the lowest values, whereas condition #3 and condition #4 achieved the highest. For UTS, condition #1, along with condition #4d, showed the lowest value, while condition #3 and condition #4b generally demonstrated the highest. In terms of elongation, condition #4 yielded the lowest values, contrasting with the highest elongation results observed in conditions #2b and #3b.

Under condition #1, the YS and UTS were the lowest compared to other conditions, even falling below the as-cast values. This decline is consistent with the hardness results and can be primarily attributed to the relatively low solution heat treatment temperature in condition #1. The primary $Mg_2Si$ phases maintained a sharp edge, and the eutectic $Mg_2Si$ were undissolved and not uniformly distributed, which negatively impacted the material's mechanical properties. As a result, YS experienced a reduction of up to 15 %.

Under condition #2, the values for YS and UTS were higher than in the previous condition. This improvement is consistent with the trend

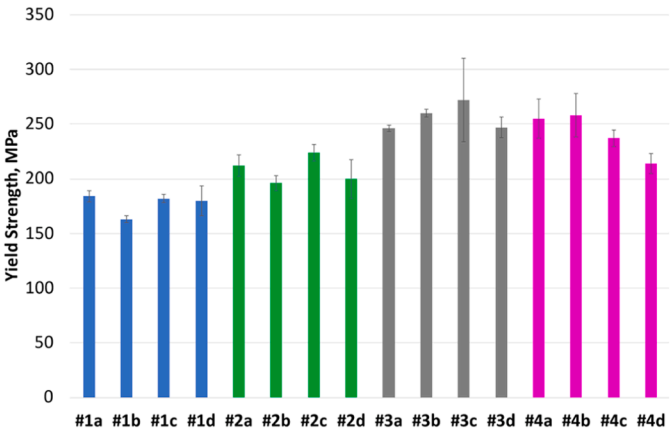


**Fig. 11.** Yield strength of HT-Al80Mg10Si5Cu5 from conditions #1 to #4 (experimental results).

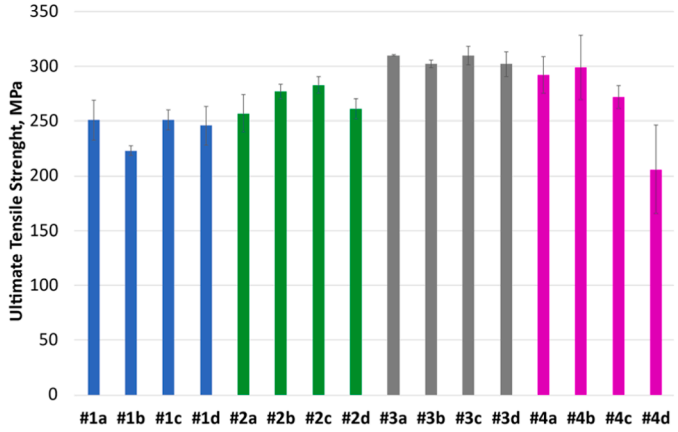


**Fig. 12.** UTS of HT-Al80Mg10Si5Cu5 from conditions #1 to #4 (experimental results).

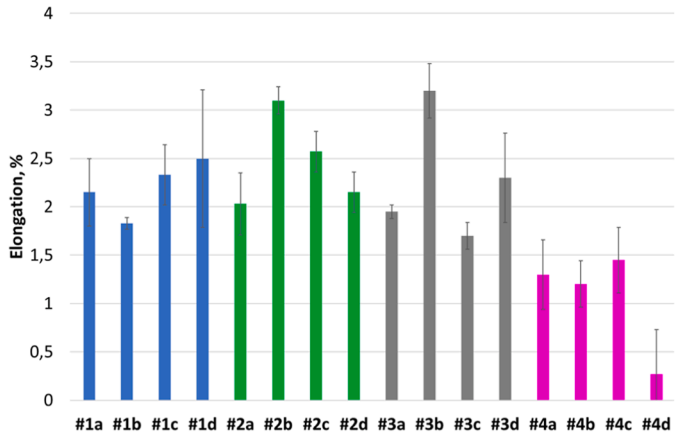


**Fig. 13.** Elongation of HT-Al80Mg10Si5Cu5 from condition #1 to #4 (experimental results).

observed for hardness, indicating that the heat treatment parameters under condition #2 were more effective in enhancing the mechanical properties. This is due to the higher solution temperature, which improves the regularity of the $Mg_2Si$ phase morphology and promotes better dissolution of the eutectic $Mg_2Si$. Under condition #2c, following the ageing process, the mechanical properties showed significant improvement, with the YS and UTS reaching the highest values under condition #2. However, the values remained approximately 30 % lower in YS and 10 % lower in UTS compared to the as-cast state. When the ageing process was carried out at 220 ºC (#2d) both YS and UTS showed a decline, indicating that the higher temperature may have led to over-ageing that reduced the alloy's strength.

Under condition #3, both the YS and UTS increased by more than 15 % compared to condition #2, reaching values comparable to those in the as-cast condition. Furthermore, elongation improved significantly, by over 80 %. This enhancement is attributed to the improved dissolution and distribution of intermetallic phases, as well as the reduction of sharp edges in primary $Mg_2Si$, which together resulted in better mechanical properties across the material. However, at an ageing temperature of 190 °C (case #3c), the elongation values dropped again by approximately 50 %. This observation can be attributed to the gradual coarsening of the microstructure, as it was seen previously.

Finally, under condition #4, the values for YS, UTS, and E were generally lower and consistent with the obtained hardness values under the same solution condition. This decrease can be attributed to the presence of coarser Cu and Mg-rich phases in the microstructure, which are detrimental to the material's mechanical properties, especially in the elongation and because of over-burning [86].

The results demonstrated that the solution treatment at the temperature of 380 ºC did not have an improved effect on tensile properties. Above this temperature value, the higher the solution temperature, the higher the YS and the UTS while the E remained approximately stable. For every 1 °C increase in solution temperature, there is approximately a 1 MPa increase in both YS and UTS, and a 5 % reduction in elongation value.

Regarding the ageing treatment, at the temperature of 160 ºC in conditions #1 and #3, the values of UTS decreased, although elongation increased. At the intermediate temperature, 190 ºC, the samples demonstrated better mechanical properties under conditions #2 and #3. In this scenario, there was an increase in YS and UTS values, however, a decrease was observed in E, which can be attributed to the restricted mobility of dislocations due to the precipitation of finer intermetallic phases [87]. When the ageing temperature value was set to 220 ºC, both the YS and UTS decreased across all conditions as the material's resistance is lower with larger intermetallic particles [88]; however, E increased by approximately 10 % in condition #1 because of the oversatured aluminium matrix, and 25 % in condition #3 due to the increased phase precipitation and gradual coarsening of intermetallic phases [78]. This increase in elongation can be attributed to the observed decrease in hardness values, that is related with an increased ductility.

It is demonstrated that condition #3 (solution temperature of 440 ºC) favoured the attainment of better values in tensile tests, with a decrease observed under condition #4 (temperatures above 460 °C). The sample subjected to condition #3a (solution temperature at 460 ºC with natural ageing process) exhibited better values for the YS/UTS ratio, while the sample subjected to condition #3b (solution temperature at 460 ºC and ageing at 160 ºC) had the best values for E.

It is worth noting, that after thermal treatment, no blisters were detected in the treated samples, as the internal porosity was low (<1.0 %) and classified as shrinkage porosity.

### 3.2.1. *Analysis of physical properties*

*3.2.1.1. Electrical conductivity.* The electrical conductivity properties of HT-samples under the different temperature conditions are given in Fig. 14. All the samples exhibited similar values; however, while the solution temperature did not significantly affect the values, they increased slightly with the ageing temperature which is consistent with findings from other studies [80,89]. It could be related to a less oversaturated Al matrix, with the morphology evolution of Si, Cu, and other alloying elements affecting the alloy's conductivity [90]. It has also been observed that samples with higher strengths (condition #3) tend to have

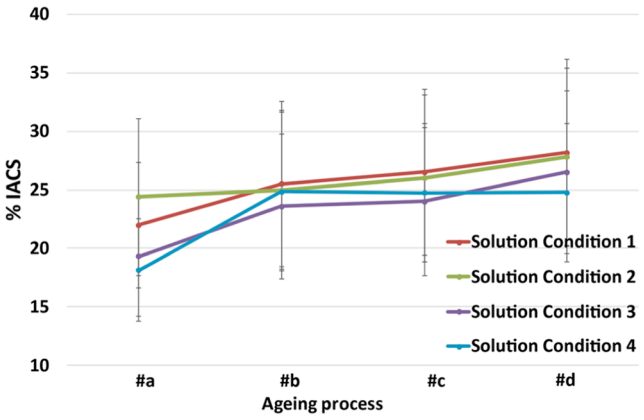


**Fig. 14.** Electrical conductivity (%IACS) depending on the thermal treatment (experimental results).

relatively lower electrical conductivity compared to those with lower strengths [91].

Compared to the as-cast samples, the electrical conductivity values increased. This enhancement is primarily attributed to the smaller concentration of Mg and Cu in the solid solution resulting from the ageing thermal treatment, which significantly increase thermal conductivity [92].

### 3.3. Results level 2

#### 3.3.1. Chemical composition and microstructure of new casting parts

The chemical composition of new casting parts is detailed in Table 7. Although the composition remained within the specified range of the Al80Mg10Si5Cu5 alloy, minor variations of less than 1 % wt. occurred during manufacturing. While the cooling rate plays a significant role, even slight changes in concentration can affect solidification reactions and the resulting microstructure [93].

When the microstructure was examined (Fig. 15), it was confirmed that a similar structure was achieved, comprising primary and eutectic $Mg_2Si$ particles, Cu-rich phases ($Al_2Cu$ and $Al_2CuMg$), and an aluminium matrix. While the sizes of the eutectic $Mg_2Si$ and aluminium dendrites were comparable to previous casting parts (3.28 ± 1.84 μm for eutectic $Mg_2Si$ and 9.04 ± 3.48 μm for aluminium), some primary $Mg_2Si$ exhibited slightly larger sizes, averaging 32 ± 19.34 μm.

The cooling curve and first derivative are shown in Fig. 16. When TA techniques were applied during the manufacture of new casting parts in level 2, it was determined that Cu-rich phases and the solidus precipitated around 3° C lower than in level 1. These small differences did not affect the parameters of the designed thermal treatments.

#### 3.3.2. Mechanical and physical properties of new casting parts in as-cast state

The mechanical and physical properties in as-cast conditions at RT were evaluated before proceeding with thermal treatments.

The hardness was recorded at 136 ± 5.0 HV3. In terms of tensile properties, the alloy exhibited a YS of 212 ± 19.5 MPa, an UTS of 258 ± 5.4 MPa, and an elongation (E) of 0.64 ± 0.3 %. The compressive strength (UCS) reached 531 ± 43.3 MPa, with a YS of 235 ± 7.0 MPa and a deformation (D) of 11.1 ± 2.3 %.

Additionally, the alloy's electrical conductivity was 18 ± 4.6 %IACS, and its density was 2.58 g/cm$^3$.

It is concluded that even a small deviation of 1 % in the chemical composition of the alloy can lead to a noticeable reduction in mechanical properties, particularly in YS under tension and compression.

#### 3.3.3. Microstructure of the HT-samples

The microstructures obtained through the selected heat treatments in level 2, under conditions #3a and #3b, are compared in Fig. 17. Also, the distribution of elements in each sample, as part of a more intensive study, can be seen in Fig. 18 and Fig. 19.

In general, both heat-treated samples displayed a more globular structure in the eutectic $Mg_2Si$ and Cu-rich phases compared to the as-cast sample.

In both conditions, Mg and Cu-rich phases were uniformly distributed throughout the aluminium matrix. In the primary $Mg_2Si$ phase, only Si and Mg were detected. The eutectic $Mg_2Si$ contained some Al, correlating with the eutectic microstructure, which consists of a mixture of Al matrix and $Mg_2Si$ precipitates. In the Cu-rich phases, both Al and Cu were identified, along with traces of Mg.

**Table 7**
Chemical composition (wt%) of new casting parts of Al80Mg10Si5Cu5 aluminium alloy manufactured in level 2 (experimental results).

| Method | Al | Mg | Si | Cu | Fe | Mn |
|---|---|---|---|---|---|---|
| OES | 79.0 | 10.3 | 5.6 | 4.7 | 0.3 | 0.1 |

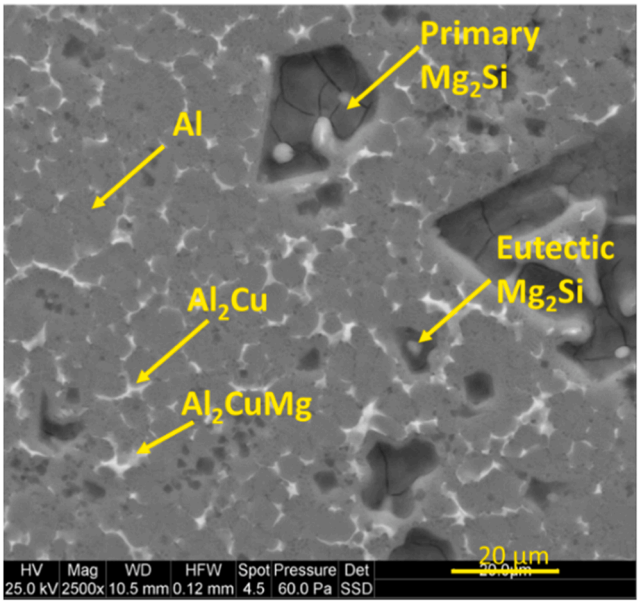


**Fig. 15.** SEM microstructure of the as-cast Al80Mg10Si5Cu5 alloy obtained in level 2.

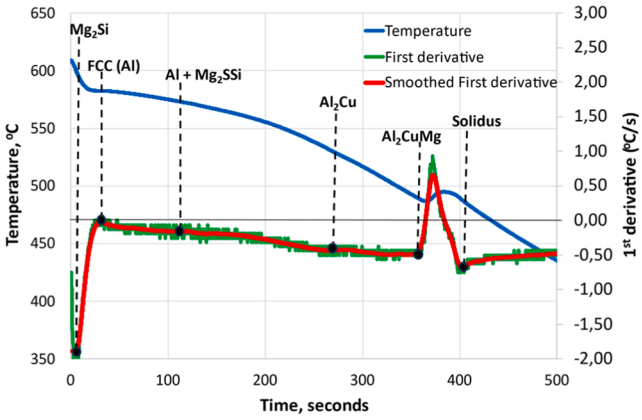


**Fig. 16.** Cooling curve and 1st derivative curves of new as-cast Al80Mg10Si5Cu5 alloy manufactured in level 2 (experimental results).

Following, the chemical composition of the different constituents in each sample was analyzed, as shown in Table 8 for case #3a and Table 9 for case #3b. It was noted that under heat treatments, the $Al_2Cu$ phase disappeared and was converted into $Al_2CuMg$. This phase is advantageous in aluminium alloys in comparison to the $Al_2Cu$ phase [94] due to its higher strength and hardness [95]. However, this phase can serve as a crack initiation source [96].

By contrasting the chemical composition of the different intermetallic, $Mg_2Si$ and $Al_2CuMg$, it was observed that under condition #3a, the $Al_2CuMg$ phase contained a smaller quantity of aluminium. However, in condition #3b, the amount of aluminium in the eutectic globular $Mg_2Si$ phase was lower.

When comparing the chemical composition of the different intermetallic of $Mg_2Si$ and $Al_2CuMg$ with various sources in the literature [97,98], it was found that the different determined phases presented a higher concentration of aluminium. This could show a better dissolution of the elements within the matrix [99].

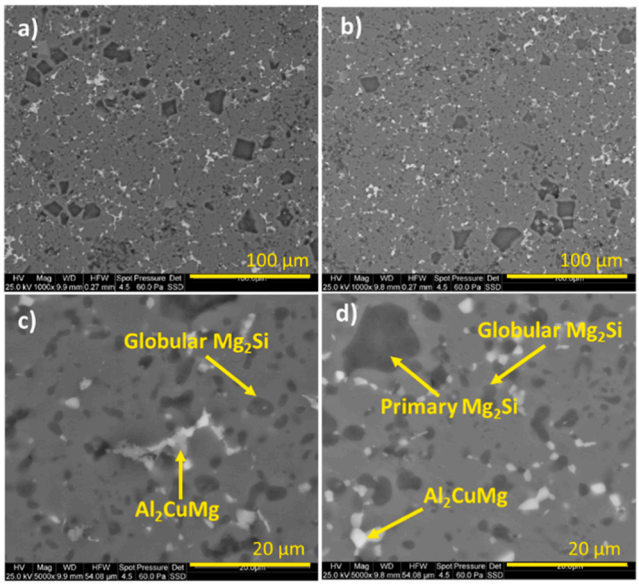


**Fig. 17.** SEM under condition #3 level 2: a) #3a x1000, b) #3b x1000, c) #3a x5000, d) #3b x5000.

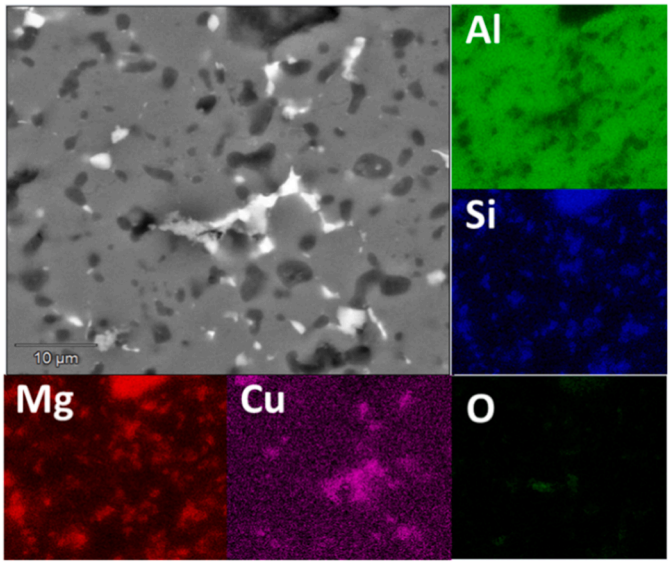


**Fig. 18.** Elemental mapping of samples subjected to condition #3a level 2.

### 3.3.4. *Mechanical properties of the thermally treated sample*

*3.3.4.1. Hardness.* The Vickers hardness values of the HT-alloy under conditions #3a and #3b, listed in Table 10, were very similar. When compared to the previous hardness data from level 1, it was observed that minor variations in the chemical composition caused a slight reduction in the hardness values. However, this decrease was less than 10 %.

### 3.4. *Tensile strength*

Table 11 presents the tensile properties under conditions #3a and #3b. It was noted that tensile properties were dissimilar to previous data obtained in level 1 for the same thermal treated conditions, and due to the geometry of new casting parts in addition to small variation in the final chemical composition. The difference in microstructure resulted in a decrease in mechanical properties. The YS and UTS dropped by up to

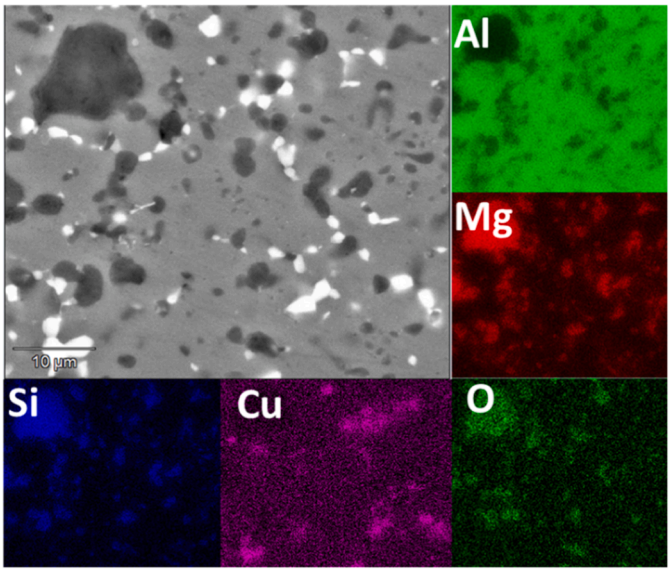


**Fig. 19.** Elemental mapping of samples subjected to condition #3b level 2.

**Table 8**
Chemical composition (wt%) of main phases under condition #3a level 2 (experimental results).

| Element | Phase | | |
|---|---|---|---|
| | **Primary $Mg_2Si$** | **Eutectic $Mg_2Si$** | **$Al_2CuMg$** |
| **Al** | 41.27 | 65.49 | 69.41 |
| **Mg** | 31.32 | 16.22 | 10.53 |
| **Si** | 23.12 | 18.29 | - |
| **Cu** | 4.29 | - | 18.13 |

**Table 9**
Chemical composition (wt%) of main phases under condition #3b level 2 (experimental results).

| Element | Phase | | |
|---|---|---|---|
| | **Primary $Mg_2Si$** | **Eutectic $Mg_2Si$** | **$Al_2CuMg$** |
| Al | 37.25 | 61.12 | 77.55 |
| Mg | 39.31 | 21.12 | 12.34 |
| Si | 25.05 | 17.76 | - |
| Cu | 1.61 | - | 10.12 |

**Table 10**
Hardness values of HT-alloy under conditions #3a and #3b level 2 (experimental results).

| Ref. | HV3 |
|---|---|
| #3a | 126 ± 6.41 |
| #3b | 128 ± 5.12 |

**Table 11**
Tensile test values HT-alloy under conditions #3a and #3b level 2 *(experimental results)*.

| Ref. | YS (MPa) | UTS (MPa) | E (%) |
|---|---|---|---|
| #3a | 221 ± 2.52 | 244 ± 4.93 | 1.1 ± 0.76 |
| #3b | 191 ± 2.83 | 229 ± 7.78 | 1.0 ± 0.28 |

25 %, while E was reduced by more than 65 %. This reduction in mechanical properties is attributed to the presence of larger primary $Mg_2Si$ particles, which negatively impacted the alloy's performance [20].

When comparing the two conditions, the YS, UTS, and E were higher for samples treated under condition #3a. This can be attributed to the differences observed in the chemical composition of intermetallic phases, where, under condition #3b, the $Mg_2Si$ phases contained a higher Mg content. This likely led to slight coarsening of some of these phases, resulting in a less uniform distribution and less refined matrix precipitation [100].

### 3.4.1. Analysis of physical properties

*3.4.1.1. Electrical conductivity.* The electrical conductivity results for the HT-Al80Mg10Si5Cu5 alloy under conditions #3a and #3b are presented in Table 12. Notably, both measurements showed nearly identical values, with a slight increase observed following the artificial ageing process. This aligns with the results obtained in level 1, where the ageing treatment had a measurable impact on the alloy's electrical conductivity, causing a slight increase.

With all these results at level 2, it was concluded that condition #3a (solution temperature at 460 ºC with natural ageing process), provided the best microstructure, mechanical and physical properties for the Al80Mg10Si5Cu5 alloy.

### 3.5. Results level 3

Finally, in phase 3, thermal treatment #3a (solution temperature of 440 ºC and natural ageing) was applied to newly manufactured samples from the previous level. These samples were subjected to a more detailed analysis, with observations made at both RT and at an elevated temperature above 200 ºC.

### 3.5.1. XRD of the HT-samples under condition #3a at RT and 200 ºC

The XRD analysis of the final HT-alloy at RT and 200 ºC is presented in Fig. 20. The results revealed the presence of aluminium, $Mg_2Si$, and $Al_2CuMg$ phases in both RT and 200 ºC. This confirms that the microstructure and phases of the new heat-treated alloy exhibited significant stability with the increase in temperature, indicating a strong thermal resistance of the alloy's phase composition under the tested conditions.

### 3.5.2. Microstructure of the HT-samples under condition #3a at RT and 200 ºC after mechanical testing

Fig. 21 and Fig. 22 show the microstructure of tensile and compressive bars tested at room temperature (RT) and at 200 ºC.

After testing at 200 °C, the $Mg_2Si$ phases and the copper-rich intermetallics ($Al_2CuMg$) remained similar in size and morphology to those observed at RT. Coalescence of $Mg_2Si$ phases was detected in only a few instances. However, the size of the precipitated phases did not increase excessively, avoiding the typical reductions in strength and hardness that occur with significant phase growth [101]. This indicated that the HT-alloy can exhibit comparable mechanical properties at RT and 200°C.

By comparing tensile and compressive specimens, it was evident that the samples tested under compression exhibited larger $Mg_2Si$ particles. This increase in particle size is attributed to the larger diameter of the specimens, which leads to a slower cooling rate.

**Table 12**
%IACS values HT-Al80Mg10Si5Cu5 under conditions #3a and #3b level 2 (experimental results).

| Ref. | %IACS |
|---|---|
| #3a | 21 ± 6.73 |
| #3b | 22 ± 6.46 |

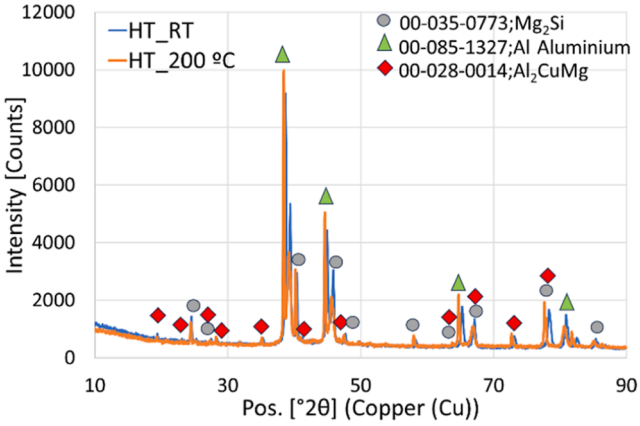


**Fig. 20.** XRD analysis of HT-Al80Mg10Si5Cu5 alloy at RT and 200 ºC (experimental results).

### 3.5.3. Fractured Surface of the HT-samples under condition #3a at RT and 200 ºC after mechanical testing

Fig. 23 and Fig. 24 illustrate the fractured surface of tensile and compressive bars tested at RT and 200 ºC.

The tensile bars displayed a mixed-mode failure, combining brittle and ductile characteristics [102]. Cleavage regions were identified, leading to brittle fracture due to the presence of hard and brittle primary $Mg_2Si$ phases [103]. Spherical cavities or dimples, indicative of ductile fracture, were also present [104], each corresponding to a void that nucleated, grew, and coalesced, with the $Mg_2Si$ serving as void initiation sites [105]. Some micro-cracks predominantly propagate in the aluminium, contributing to premature fracture [106].

In the case of the compression bars, a different behaviour was observed, characterized by a ductile fracture. This fracture featured dimples with a unique structure, including parabolic or elongated shapes that indicated significant plastic deformation due to shear stress [107]. Additionally, regions with tearing were noted, suggesting the formation of ridges at the fracture ends after maximum deformation. The presence of dispersed particles in the fracture zones, typical of ductile fractures, was also detected [102].

### 3.5.4. Mechanical properties of the HT-samples under condition #3a at RT and 200 ºC

*3.5.4.1. Hardness.* The Vickers hardness values of HT- alloys under condition #3a at RT and 200 ºC are listed in Table 13. Also, the effects of two additional temperatures (250 ºC and 300 ºC) were investigated on hardness properties to confirm a suitable operating temperature.

The results indicated that extending the solution time from 24 to 72 hours and quenching in hot water, yielded consistent hardness values. When the temperature was increased to 200 ºC, there was a slight decrease in hardness of approximately 10 % as a consequence of relieving the effects of residual stresses [22]. When subjected to higher temperatures from 250 ºC onwards, the hardness values remained stable, slightly higher than those at 200ºC, possibly due to secondary finer precipitation hardening [22,108]. However, at 300 ºC, the hardness values decreased, likely due to the continued coalescence of $Mg_2Si$ phases within the Al matrix, contributing to alloy softening [21,109].

Notably, the hardness value at 200ºC remains more than 60 % higher than the value reported in other studies [21].

*3.5.4.2. Tensile strength.* The tensile properties under condition #3a at RT and 200 ºC are listed in Table 14. In this case, tensile properties at temperatures of 250 ºC and 300 ºC were also analyzed.

The results confirmed that extending the solution time from 24 to 72 hours and quenching in hot water, enhanced the tensile properties,

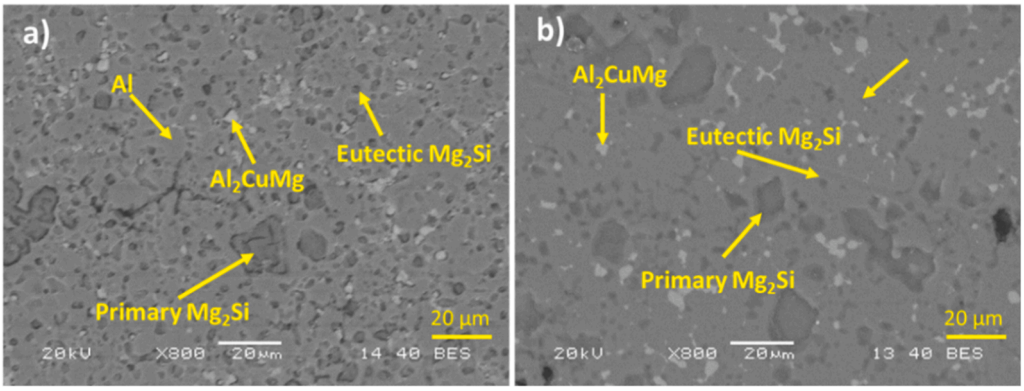


**Fig. 21.** x800 SEM of the HT- tensile tested bars under condition #3a: a) at RT, b) at 200 ºC.

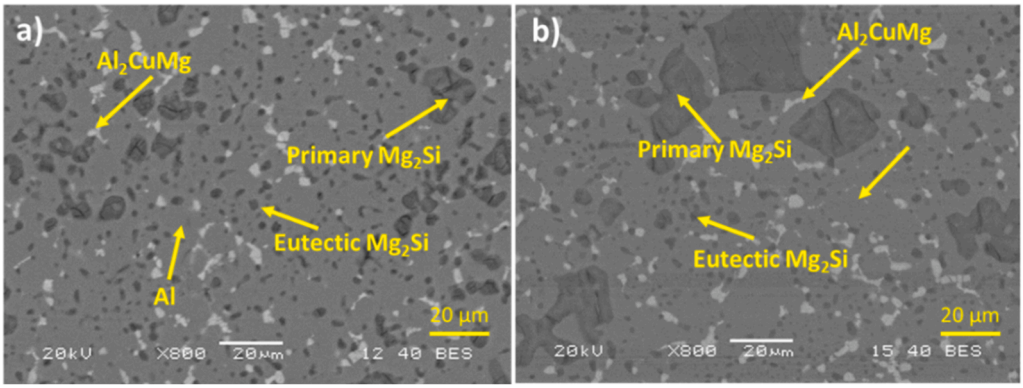


**Fig. 22.** x800 SEM of the HT-compressive tested bars under condition #3a: a) at RT, b) at 200 ºC.

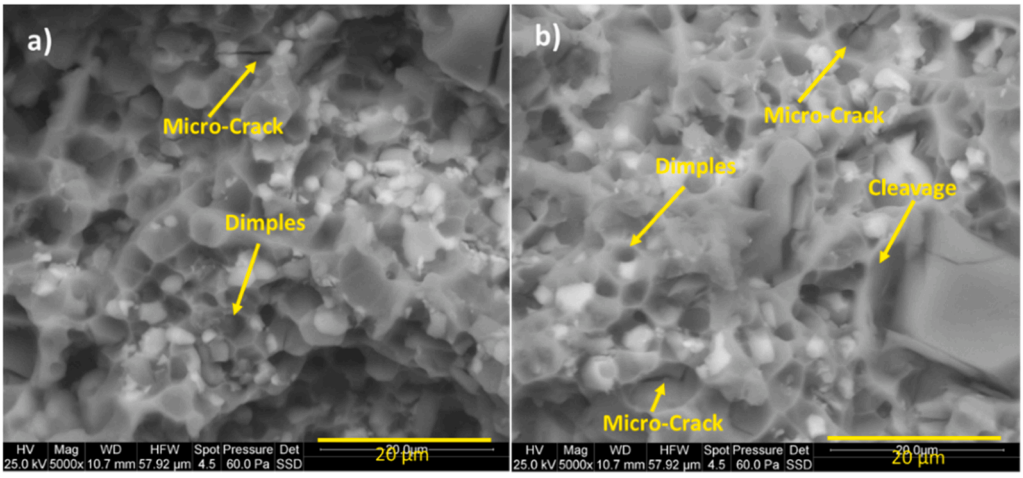


**Fig. 23.** x5000 SEM from the fracture of HT-tensile tested bars: a) at RT, b) at 200ºC.

leading to increases of approximately 5 MPa in YS and 10 MPa in UTS, respectively.

At 200 ºC, YS and E showed a minimal temperature sensitivity, with the UTS decreasing by only 6 %. While the alloy displayed reduced YS and UTS at higher temperatures, contrary to other literature [18,110], reporting significant strength loss and increased ductility beyond 150 °C, this study indicates that the new heat-treated alloy maintained excellent tensile properties up to 200 ºC.

*3.5.4.3. Compressive strength.* The compressive properties under condition #3a at RT and 200 ºC are listed in Table 15.

The main reason for the superior ductility during compression tests than tensile tests could be attributed to that casting pores have a significantly detrimental impact on tensile properties preventing crack propagation [111].

When comparing the results with the as-cast samples, the UCS values increased by approximately 20 %. However, the YS was slightly lower, by about 7 %, while D improved by around 60 %. At 200 °C, the YS decreased by less than 3 %, the UCS dropped by approximately 30 %, and the D reduced by around 10 %.

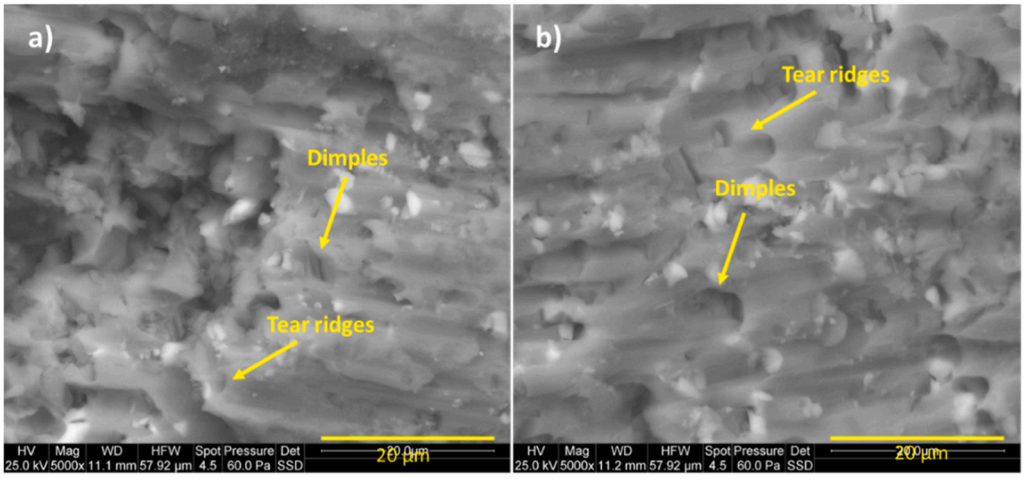


**Fig. 24.** x5000 SEM from the fracture of heat-treated compressive test bars: a) at RT, b) at 200ºC.

**Table 13**
Hardness values of HT-alloy under condition #3a at RT and high temperature (experimental results).

| Temperature | HV3 |
|---|---|
| 25 ºC | 128 ± 3.85 |
| 200 ºC | 114 ± 0.57 |
| 250 ºC | 125 ± 4.16 |
| 300 ºC | 117 ± 4.16 |

**Table 14**
Tensile test values of HT-Al80Mg10Si5Cu5 alloy under condition #3a at room and high temperature *(experimental results)*.

| Temperature | YS (MPa) | UTS (MPa) | E (%) |
|---|---|---|---|
| 25 ºC | 226 ± 10.85 | 254 ± 11.10 | 1.00 ± 0.10 |
| 200 ºC | 226 ± 5.93 | 238 ± 6.38 | 1.00 ± 0.25 |
| 250 ºC | 107 ± 25.5 | 194 ± 9.02 | 2.06 ± 0.28 |
| 300 ºC | 95 ± 10.6 | 168 ± 10.61 | 3.15 ± 0.92 |

**Table 15**
Compressive test values of HT-Al80Mg10Si5Cu5 alloy at RT and 200 ºC *(experimental results)*.

| Temperature | YS (MPa) | UCS (MPa) | D (%) |
|---|---|---|---|
| 25 ºC | 217 ± 8.89 | 665 ± 22.610 | 28.20 ± 4.29 |
| 200 ºC | 211 ± 6.35 | 468 ± 15.10 | 25.31 ± 2.56 |

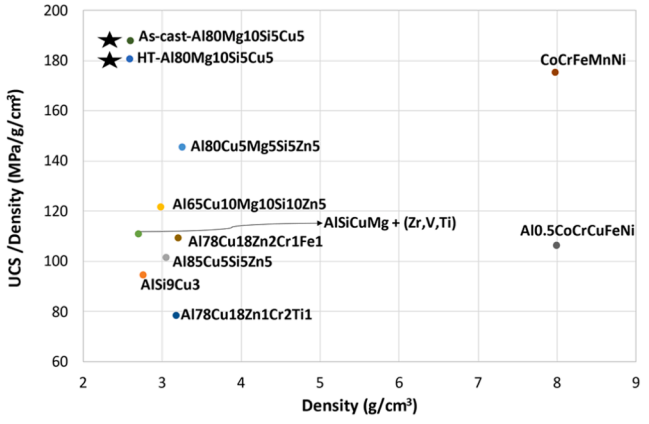


**Fig. 25.** Compressive strength-density diagram at 200 ºC.

To assess the compressive strength of the newly developed Al80Mg10Si5Cu5 alloy against other multi-component aluminium alloys reported in the literature, Fig. 25 illustrates a plot of compressive strength versus density. This plot includes the AlSi9Cu3 alloy and various multi-component aluminium alloys such as Al85Cu5Si5Zn5, Al65Cu10Mg10Si10Zn5, Al80Cu5Mg5Si5Zn5 [112], among others [24, 25,113–115]. Notably, the new Al80Mg10Si5Cu5 alloy, both in as-cast and heat-treated conditions (marked with stars in Fig. 25), shows the best balance between density and compressive strength at 200 ºC.

## 4. Conclusions

In the present research, a heat treatment (HT) for a new patented multi-component Al80Mg10Si5Cu5 aluminium alloy has been developed. The optimal HT was determined as the solution at 440 ºC solution time of 72 hours, quenched in hot water at the temperature of 75 ºC, and natural ageing. Extending the solution time from 24 to 72 hours and quenching in hot water improved tensile values by around 5 %.

The alloy's tensile strength was significantly improved, with the E increasing by around 40 % and YS around 14 MPa, while the UTS remained stable, with the UCS increasing by around 20 % and D by around 60 % The YS reduced by less than 10 %. Electrical conductivity was improved by approximately 15 %.

At 200 ºC the tensile properties remained near constant. The UCS dropped by approximately 30 %, while YS and D remained nearly constant.

The enhanced properties observed after thermal treatments can be directly linked to the transformation of the $Al_2Cu$ phase into the $Al_2CuMg$ phase, which plays a key role in strengthening the alloy. This transformation not only contributes to improved hardness and tensile strength but also positively influences the alloy's overall microstructural stability and resistance to deformation.

These findings highlight the alloy's performance, indicating that the Al80Mg10Si5Cu5 alloy offers one of the best ratios of compressive strength to density among multi-component alloys, particularly at elevated temperatures. Noticeably, the ductility under tension and compression was significantly improved.

Future research will focus on investigating the effects of varying solutions and ageing times on the alloy's properties. This will help to further optimize mechanical performance, particularly to understand how these factors influence microstructure stability and strength at different temperatures.

## CRediT authorship contribution statement

**Ester Villanueva:** Writing – original draft, Investigation. **Iban Vicario:** Writing – review & editing, Investigation, Methodology, Funding acquisition. **Ignacio Crespo:** Writing – original draft, Investigation. **Teresa Guraya:** Writing – review & editing, Conceptualization, Supervision. **Iñaki Hurtado:** Writing – review & editing, Investigation, Supervision. **Joseba Albizuri:** Writing – review & editing, Investigation, Conceptualization, Project administration, Supervision.

## Declaration of Competing Interest

The authors declare the following financial interests/personal relationships which may be considered as potential competing interests: Iban Vicario reports financial support was provided by Tecnalia Research & Innovation Foundation. Iban Vicario, Ester Villanueva, Joseba Albizuri, Teresa Guraya has patent #EP23383372.2 pending to TECNALIA & EUSKAL HERRIKO UNIBERTSITATEA. If there are other authors, they declare that they have no known competing financial interests or personal relationships that could have appeared to influence the work reported in this paper.

## Acknowledgement

This work has been partially funded by the Basque Government through the IT1542-22, ELKARTEK KK-2022/00082 (MINERVA), and KK-2023/00020 (DESGAS).

## Data availability

Data will be made available on request.

## References

[1] T. Trzepiecinski, S.M. Najm, Current Trends in Metallic Materials for Body Panels and Structural Members Used in the Automotive Industry, Materials 17 (2024) 590, https://doi.org/10.3390/ma17030590.
[2] Kie Soo, V. Peeters, J. Paraskevas, D. Compston, P. Doolan, M. Duflou, J. Sustainable aluminium recycling of end-of-life products: A joining techniques perspective, J. Clean. Prod. (2018) 128–132, https://doi.org/10.1016/j.jclepro.2017.12.235.
[3] The average weight of passenger cars in Europe has increased significantly since 2020. Available online: ⟨https://www.inovev.com/index.php/en/market-analyses/category-blog/19969-2023-30-2⟩.
[4] Aluminum Content in Passenger Vehicles (Europe). Available online:⟨https://european-aluminium.eu/wp-content/uploads/2023/05/23-05-02Aluminum-Content-in-Cars_Public-Summary.pdf⟩.
[5] J.F. Nie, A.J. Morton, B.C. Muddle, Automotive Trends in Aluminium - The European Perspective, Proc. 9th Int. Conf. Alum. Alloy. (2004) 15–23.
[6] Aluminum Content in Cars, Summary Report 2016. Available Online: ⟨https://www.alfed.org.uk/files/Fact%20sheets/european-aluminium-ducker-study-summary-report_sept.pdf⟩.
[7] By 2030, cars will be using much more aluminium than today – and other trends. Available Online: ⟨https://www.shapesbyhydro.com/en/manufacturing/by-2030-cars-will-be-using-much-more-aluminium-than-today–and-other-trends/⟩.
[8] Aluminium usage in cars surges as automotive industry shifts towards electrification. European Aluminium. Available online: ⟨https://aluminiumtoday.com/news/aluminium-usage-in-cars-surges-as-automotive-industry-shifts-towards-electrification⟩.
[9] F. Czerwinski, Current trends in automotive lightweighting strategies and materials, Materials 14 (21) (2021) 6631, https://doi.org/10.3390/ma14216631.
[10] US7762622B2. Structural member for a motor vehicle.
[11] Avci-Karatas C. Examination of aluminum alloy usage in structural engineering. 4th International Black Sea Modern Scientific Research Congress. 2023.
[12] D. Lehmhus, Advances in Metal casting technology: a review of state of the art, challenges and trends—part i: changing markets, changing product, Metals 12 (11) (2022) 1959, https://doi.org/10.3390/met12111959.
[13] P. Mulidrán, E. Spisak, Production of large car body parts with the use of die-casting technology – Giga pres, Transf. Innov. 48 (2013) 4.
[14] Baser T., Umay E., Akinci V. New Trends in Aluminum Die Casting Alloys for Automotive Applications. International Conference on Technology. 2022. Lecture notes in EPSTEM 2022;21:79.
[15] J. Hajkowski, P. Popielarski, R. Sika, Prediction of HPDC casting properties made of AlSi9Cu3 alloy, Adv. Manuf. (2018) 621, https://doi.org/10.1007/978-3-319-68619-6_59.
[16] Vicario I., Anza I., Sáenz De Tejada F., García J.C., Galarraga H., Merchan M. Development of new Al-Si9Cu3 alloys for HPDC components with tailored properties. 71st World Foundry Congress: Advanced Sustainable Foundry. WFC 2014. Bilbao.
[17] S. Sulardjaka, S. Nugroho, N. Iskandar, Mechanical properties of AlSiMg/SiC and AlSiMgTiB/SiC produced by semi-solid stir casting and high pressure die casting, Mater. Phys. Mech. 031 (2021), https://doi.org/10.18149/MPM.4712021_3.
[18] Market Development for secondary Casting Alloys beyond Motor Blocks - Study on casting alloy market and recycling. 2023. Technical report 2023. Available online: https://international-aluminium.org/wp content/uploads/2023/07/IRT_M2P_Market-Development-for-2ary-Casting-Alloys-beyond-Motor-Blocks_final.pdf
[19] A. Zovi, F. Casarotto, Silafont-36, the low iron ductile die casting alloy development and applications, La Metall. Ital. 33 (2007).
[20] A. Shafieizad, A.Z. Hanzaki, H.R. Abedi, Al-Fadhlah KJ, The $Mg_2Si$ phase evolution during thermomechanical processing of in-situ aluminium matrix macro-composite, Mater. Sci. Eng. A 664 (2015) 310–317, https://doi.org/10.1016/j.msea.2015.07.060.
[21] NADCA Product Specification Standards for Die Casting. Die Casting handbook. NADCA, Nadca publication #G200.
[22] E. Garibaldi, J.N. Lemke, L. Rovatti, O. Baer, G. Timelli, F. Bonollo, High-temperature behavior of high-pressure diecast alloys based on the Al-Si-Cu system: the role played by chemical composition, Metals 8 (5) (2018) 348, https://doi.org/10.3390/met8050348.
[23] G. Timelli, A. Fabrizi, S. Vezzu, A. De Mori, Design of wear-resistant diecast AlSi9Cu3(Fe) alloys for high-temperature components, Metals 10 (1) (2019) 55, https://doi.org/10.3390/met10010055.
[24] M. Zamani, S. Seifeddine, A.E.W. Jarfors, High temperature tensile deformation behavior and failure mechanisms of an Al-Si-Cu-Mg cast alloy – the microstructural scale effect, Mater. Des. 86 (2015) 361–370, https://doi.org/10.1016/j.matdes.2015.07.084.
[25] F. Czerwinski, W. Kasprzak, D.G. Sediako, D. Emadi, S.K. Shaha, J. Friedman, D. Chen, Development of high temperature aluminum alloys for automotive powertrain, AMP Tech. Artic. 174 (3) (2016) 16–20, https://doi.org/10.31399/asm.amp.2016-03.p016.
[26] V. Balaji, X. Anthony, Development of high entropy alloys (HEAs): current trends, Heliyon 10 (2024) e26464, https://doi.org/10.1016/j.heliyon.2024.e26464.
[27] H. Adil, F. Audebert, F. Saporiti, S. Gerguri, F. Bonatesta, J.F. Durodola, Microstructure and mechanical properties of an Al-Mg-Si-Cu alloy, Mater. Sci. Res. India 20 (3) (2023) 154, https://doi.org/10.13005/msri/200303.
[28] Shu M. Methods to Improve the Performance of Aluminum Alloy. IOP Conference Series Earth and Environmental Science 2021;783: 012053. https://doi.org/10.1088/1755-1315/783/1/012053.
[29] Z. Yuan, Z. Guo, S.M. Xiong, Skin layer of A380 aluminium alloy die castings and its blisterin during solution treatment, J. Mater. Sci. Technol. 35 (9) (2019) 1906–1916, https://doi.org/10.1016/j.jmst.2019.05.011.
[30] G. Sigworth, R.J. Donahue, The metallurgy of aluminum alloys for structural high pressure die castings, Int. J. Met. 15 (3) (2021) 1031.
[31] Roos, H.J.; Lagler, M.; Quintana, L. Whitepaper: Die Zukunft von Strukturbauteilen für Druckgusslösungen. Bühler AG, 2019. Available online: ⟨https://assetcdn.buhlergroup.com/asset/874601345621/86bd505f19e643b2b3ce79957169681c⟩.
[32] G. Soares, R. Neto, R. Madureira, R. Soares, J. Silva, R. Silva, L. Araujo, Characterization of Al alloys injected through vacuum-assisted HPDC and influence of T6 heat treatment, Metals 13 (2) (2023) 389, https://doi.org/10.3390/met13020389.
[33] A.M.A. Mohamed, F.H. Samuel, A review on the heat treatment of Al-Si-Cu/Mg casting alloys, Heat. Treat. - Conv. Nov. Appl. 4 (2012) 55, https://doi.org/10.5772/50282.
[34] Q. Yan, Y. Qiu, M. Yang, Q. Lu, H. Lin, M. Yang, K. Li, Y. Du, Effects of rapid quenching on grain boundary microstructure and mechanical properties of an Al-Mg-Si-Cu alloy, Mater. (Basel) 16 (2023) 5609, https://doi.org/10.3390/ma16165609.
[35] S.W. Dean, G. Sanchez, C. Bronzini, A.C. Canale, L.C.F. Canale, G. Totten, Water and polymer quenching of aluminum alloys: a review of the effect of surface condition, water temperature, and polymer quenchant concentration on the yiel strength of 7075-T6 aluminum plate, J. ASTM Int. 6 (1) (2008), https://doi.org/10.1520/JAI102098.
[36] Z. Yang, J. Banhart, Natural and artificial ageing in aluminium alloys – the role of excess vacancies, Acta Mater. 215 (2021) 117014, https://doi.org/10.1016/j.actamat.2021.117014.
[37] Y.S. Yu, Y. Pei, X. Yan, F. Li, Y. Wu, S. Liu, On the Guinier-Preston zones in selective laser melted AlSi10Mg alloy, Mater. Today Commun. 38 (2024) 108508, https://doi.org/10.1016/j.mtcomm.2024.108508.
[38] W. Reif, S. Yu, J. Dutkiewicz, R. Cianh, J. Krol, Pre-ageing of AlSiCuMg alloys in relation to structure and mechanical properties, Mater. Des. 18 (4) (1997) 253, https://doi.org/10.1016/S0261-3069(97)00060-5.
[39] S. Menargues, E. Martin, M.T. Baile, J.A. Picas, New short T6 heat treatments for aluminium silicon alloys obtained by semisolid forming, Mater. Sci. Eng.: A 621 (2015) 236, https://doi.org/10.1016/j.msea.2014.10.078.
[40] S. Menargues, M.T. Baile, Alonso AF. Nuevos tratamientos T6 para aleaciones de AlSi obtenidas por conformación en estado semisólido, Rev. De. Metal. 49 (2013) 266.
[41] S.K. Tang, T. Sritharan, Morphology of beta-AlFeSi intermetallic in Al-7Si alloy castings, Mater. Sci. Technol. 14 (8) (1998) 738.

[42] L. Pedersen, L. Arnberg, The effect of solution heat treatment and quenching rates on mechanical properties and microstructures in AlSiMg foundry alloys, Metall. Mater. Trans. A 32 (2001) 525.

[43] R. Lumley, R.G. ODonell, D. Gunasegaram, M. Givord, Heat treatment of high-pressure die castings, Metall. Mater. Trans. A 38 (10) (2007) 2564, https://doi.org/10.1007/s11661-007-9285-4.

[44] J.Castings Campbell, The new metallurgy of cast metals, Butterworth Heinemann Ltd, Oxford, United Kingdom, 2003.

[45] J.F. Alvarez, E. Segurado, H. Neira, J. Asensio, Heat treatment optimization in Al-Cu-Mg-Si alloys, with or without prior deformation, Metals 8 (10) (2018) 739, https://doi.org/10.3390/met8100739.

[46] G. Timelli, O. Lohne, L. Arnberg, H.I. Laukli, Effect of solution heat treatments on the microstructure and mechanical properties of a Die-Cast AlSi7MgMn alloy, Metall. Mater. Trans. A 39 (7) (2008) 1747, https://doi.org/10.1007/s11661-008-9527-0.

[47] E. Sjolander, S. Seifddine, The heat treatment of Al-Si-Cu-Mg casting alloys, J. Mater. Process. Technol. 210 (10) (2010) 1249, https://doi.org/10.1016/j.jmatprotec.2010.03.020.

[48] A. Loizaga, E. De La Fuente, A. Niklas, A.I. Fernandez-Calvo, Optimización de las propiedades mecánicas de las aleaciones AlSi7Mg moldeadas en arena, Rev. De. Metal. 46 (2010) 64.

[49] K. Ragab, Mechanical characterisation and quality index of A356-type aluminium castings heat treated using fluidised bed quenching, Mater. Sci. Technol. 29 (4) (2012) 412, https://doi.org/10.1179/1743284712Y.0000000124.

[50] F. Bosio, P. Fino, D. Manfredi, M. Lombardi, Strengthening strategies for an Al alloy processed by in-situ alloying during laser powder bed fusion, Mater. Des. 212 (2021) 110247, https://doi.org/10.1016/j.matdes.2021.110247.

[51] G. Wang, Q. Sun, L. Feng, L. Hui, C. Jing, Influence of Cu content on ageing behavior of AlSiMgCu cast alloys, Mater. Des. 28 (3) (2007) 1001, https://doi.org/10.1016/j.matdes.2005.11.015.

[52] J.A. Santamaría, J. Sertucha, A. Redondo, I. Lizarralde, E. Ochoa de Zabalegui, P. Rodríguez, Towards the prediction of tensile properties in automotive cast parts manufactured by LPDC with the A356.2 alloy, Metals 12 (4) (2022) 656, https://doi.org/10.3390/met12040656.

[53] Q. Qi, M. Li, Y. Duan, H. Bu, Mengnie L, effect of solution heat treatment on the microstructure and microhardness of 7050 aluminum alloy, Metals 13 (11) (2023) 1819, https://doi.org/10.3390/met13111819.

[54] M.A. Azmah, S. Chang, O. Khang, Effect of a two-step solution heat treatment on the microstructure and mechanical properties of 332 aluminium silicon cast alloy, Mater. Des. 32 (4) (2011) 2334, https://doi.org/10.1016/j.matdes.2010.12.040.

[55] B. Xiao, Q. Wang, P. Jadhav, K. Li, An experimental study of heat transfer in aluminum castings during water quenching, J. Mater. Process. Technol. 210 (4) (2010) 2023–2028, https://doi.org/10.1016/j.jmatprotec.2010.07.026.

[56] M. Abdi, S.G. Shabestari, Novel high strength Al−10.5Si−3.4Cu−0.2Mg alloy produced through two-stage solution heat treatment, Trans. Nonferrous Met. Soc. China 31 (2021) 576, https://doi.org/10.1016/S1003-6326(21)65520-6.

[57] L. Xiao, H. Yu, Y. Qin, G. Liu, Z. Peng, X. Tu, H. Su, Y. Xiao, Q. Zhong, S. Wang, Z. Cai, X. Zhao, Microstructure and mechanical properties of cast Al-Si-Cu-Mg-Ni-Cr alloys: effects of time and temperature on two-stage solution treatment and ageing, Mater. (Basel) 16 (7) (2023) 2675, https://doi.org/10.3390/ma16072675.

[58] C. Seok, S. Guy, W. Sik, Two-step solution heat treatment of AlSiCu alloy for improvement of mechanical properties, Mater. Sci. Forum 857 (2016) 246, https://doi.org/10.4028/www.scientific.net/MSF.857.246.

[59] S. Toschi, Optimization of A354 Al-Si-Cu-Mg alloy heat treatment: effect on microstructure, hardness, and tensile properties of peak aged and overaged alloy, Metals 8 (11) (2018) 961, https://doi.org/10.3390/met8110961.

[60] O.S. Es-Said, D. Lee, W.D. Pfost, D.L. Thompson, M. Patterson, J. Foyos, R. Marloth, Alternative heat treatments for A357-T6 aluminum alloy, Eng. Fail. Anal. 9 (1) (2002) 99, https://doi.org/10.1016/S1350-6307(00)00034-0.

[61] A. Assadiki, V.A. Esin, M. Bruno, R. Martinez, Stabilizing effect of alloying elements on metastable phases in cast aluminum alloys by CALPHAD calculations, Comput. Mater. Sci. 34 (2018) 1, https://doi.org/10.1016/j.commatsci.2017.12.056.

[62] M. Zamani, Toshi S. Morri, A. Ceschini, L. Seifeddine, S. Optimisation of heat treatment of Al–Cu–(Mg–Ag) cast alloys, J. Therm. Anal. Calorim. 139 (2020) 3427, https://doi.org/10.1007/s10973-019-08702-x.

[63] Y. Vahidshad, A.H. Khodabakhshi, Effect of solution treatment and ageing temperature on α′ and Ti 3Al(α2) phase formation and mechanical properties of water-quenched Ti–6Al–4V, Metallogr. Microstruct. Anal. 11 (2022) 59, https://doi.org/10.1007/s13632-021-00818-7.

[64] M.B. Djurdjevic, I. Vicario, G. Huber, Review of thermal analysis applications in aluminium casting plants, Rev. De. Metal. 50 (1) (2013) e004, https://doi.org/10.3989/revmetalm.004.

[65] I. Vicario, E. Villanueva, J. Montero, M. Djurdjevic, The determination of dendrite coherency point characteristics using three new methods for aluminum alloys, Appl. Sci. 8 (8) (2018) 136, https://doi.org/10.3390/app8081236.

[66] E. Villanueva, I. Vicario, J.M. Sanchez, J. Albizuri, J. Montero, Solid fraction determination at the rigidity point by advanced thermal analysis, Appl. Sci. 12 (1) (2021) 237, https://doi.org/10.3390/app12010237.

[67] Y. Li, Q. Wang, Intelligent evaluation of melt iron quality by pattern recognition of thermal analysis cooling curves, J. Mater. Process. Technol. 161 (3) (2005) 430–434.

[68] Cehiz K., Cooling curve thermal analyses and oxygen activity analyses for the estimation of microstructural properties of nodular cast iron, Thesis Master of Science in Metallurgical and Materials Engineering Department, Middle East Technical University 2019.

[69] S. Gain, Mechanical characterization of the AlSi9Cu3 cast alloy under distinct stress states and thermal conditions, Eng. Fract. Mech. 216 (2019) 106499. ⟨https://doi.org/10.1016/j.engfracmech.2019.106499⟩.

[70] E. Rincon, H.F. Lopez, M. Cisneros, H. Mancha, Temperature effects on the tensile properties of cast and heat treated aluminum alloy A319, Mater. Sci. Eng. A 519 (1-2) (2009) 128, https://doi.org/10.1016/j.msea.2009.05.022.

[71] Y. Shengli, J. Shen, Y. Xiaodong, L. Xiwu, Z. Fei, S. Baoqing, Homogenization treatment parameter optimization and microstructural evolution of Al-Cu-Li alloy, Rare Met. Mater. Eng. 46 (1) (2017) 0028, https://doi.org/10.1016/S1875-5372(17)30072-3.

[72] A.A. Bogno, J. Valloton, D.D. Jimenez, M. Rappaz, H. Henein, Rapid solidification of Al-Cu droplets of near eutectic composition, IOP Conf. Ser.: Mater. Sci. Eng. 529 (2019) 012021, https://doi.org/10.1088/1757-899X/529/1/012021.

[73] Mackenzie S. Heat treatment of aluminum, part II: Water quenching. Thermal processing 2020. Available online: ⟨https://thermalprocessing.com/heat-treatment-of-aluminum-part-ii-water-quenching/⟩.

[74] H. Dong, S. Xiang, J. Lv, Y. Wang, L. Li, W. Yu, Modification of Mg2Si phase morphology in Mg-4Si alloy by Sb and Nd additions, J. Mater. Eng. Perform. 26 (6) (2020), https://doi.org/10.1007/s11665-020-04812-y.

[75] S. Saha, S. Hossain, R. Hasan, B. Rashid, Effect of overageing conditions on microstructure and mechanical properties in Al–Si–Mg alloy, Am. J. Eng. Res. (AJER) 5 (11) (2016) 321.

[76] Kumar H. Effect of Solution Treatment on the Hardness and Tensile Properties of Al–Mg–Si Alloys for Automotive Chassis, Mater. Trans. 60 (5) (2019) 815.

[77] A. Tsepeleva, P. Novak, E. Kolesnichenko, A. Michalcova, Z. Kacenka, J. Kubasek, Heat treatment of aluminum alloys with the natural combination of dopant, Mater. (Basel) 15 (16) (2022) 5541, https://doi.org/10.3390/ma15165541.

[78] G.D. Jiang, Y.H. Cai, Qui C. Zhang, W.W. Zhang, DT, Effect of over-aging on the microstructure, mechanical properties and crashing performance of thin-walled Al-Mg-Si-Cu alloy profiles, J. Mater. Res. Technol. 21 (21) (2022), https://doi.org/10.1016/j.jmrt.2022.10.137.

[79] X. Guo, J. zhang, X.M. Zhang, Effect of grain boundary on the precipitation behavior and hardness of Al- Cu-Mg alloy bicrystals during stress-aging, Mater. Sci. Eng.: A 683 (2017) 129–134, https://doi.org/10.1016/j.msea.2016.12.002.

[80] V.A. Medrano, E. Arrieta, J. merino, B. Ruvalcaba, K. Caballero, B. ramirez, J. Diemann, L. Murr, R.B. Wicker, D. Godfrey, M. benedict, F. Medina, A comprehensive and comparative study of microstructure and mechanical properties for post-process heat treatment of AlSi7Mg alloy components fabricated in different laser powder bed fusion systems, J. Mater. Res. Technol. 24 (2) (2023), https://doi.org/10.1016/j.jmrt.2023.04.129.

[81] M. Panuskova, E. Tillova, M. Chalupova, Relation between mechanical properties and microstructure of cast aluminum alloy AlSi9Cu3, Strength Mater. 40 (1) (2008) 98–101.

[82] P. Singh, D.X.T. George, A.A. Joe, G.A. Raja, Effect of heat treatment on the hardness behaviour of the aluminium 6061 alloy, Mater. Today Proc. 2214 (2023), https://doi.org/10.1016/j.matpr.2023.02.345.

[83] S. Zahid, Improved tensile strength and electrical conductivity of the electrical conductor aluminum alloy 6201. SME 2021 international mechanical engineering congress and exposition 2021. Lecture notes in, J. Mater. Sci., Met. Corros. (2020), https://doi.org/10.1007/s10853-020-04849-3.

[84] G.D. Jiang, Y. Cai, C. Qiu, W.W. Zhang, D.T. Zhang, Effect of over-ageing on the microstructure, mechanical properties and crashing performance of thin-walled Al-Mg-Si-Cu alloy profiles, J. Mater. Res. Technol. 21 (2022) 3074, https://doi.org/10.1016/j.jmrt.2022.10.137.

[85] P. Ren, C. Zhao, Z. Zuo, Y. Shui, D. Li, W. Huang, Effect of thermal degradation on mechanical properties of cast Al-Si alloys for cylinder heads, Eng. Fract. Mech. (2023) 109200, https://doi.org/10.1016/j.engfracmech.2023.109200.

[86] M. Liang, L. Chen, G. Zhao, Y. Guo, Effects of solution treatment on the microstructure and mechanical properties of naturally aged EN AW 2024 Al alloy sheet, J. Alloy. Compd. 824 (2020) 153943, https://doi.org/10.1016/j.jallcom.2020.153943.

[87] B.N. Sharath, D.G. Pradeep, K.S. Madhu, A review on the potential impact of age hardening on aluminium alloys and hybrid composites for engineering applications, Prog. Eng. Sci. 1 (2-3) (2024) 100013, https://doi.org/10.1016/j.pes.2024.100013.

[88] Heat treatment of aluminium VI – Artificial aging. Available online: ⟨https://thermalprocessing.com/heat-treatment-of-aluminum-vi-artificial-aging/⟩.

[89] Mondal C. Correlations between electrical conductivity and ageing behaviour of 7010 base aluminium alloys. International Conference on Aluminium (INCAL'03) 2003. Lecture notes in: Proceedings of the International Conference on Aluminium 2003;255.

[90] Zhang L., Liao H., Li J., Tang L., Investigation on Heat Treatment Process Optimization of Super-Slow- Speed Die Casting A356.2 Alloy. WFC 2024, 3-High entropy Alloys;251-253.

[91] Y. Yang, J. Nie, Q. Mao, Y. Zhao, Improving the combination of electrical conductivity and tensile strength of Al 1070 by rotary swageing deformation, Results Phys. 13 (2019) 102236, https://doi.org/10.1016/j.rinp.2019.102236.

[92] Y. Liu, Y. Zhang, W. Liu, X. Jiao, H. Nishat, D. Ajavavarakula, H. Chen, S. Xiong, Enhanced mechanical properties and thermal conductivity of high-pressure die-cast AlMg6Si2MnZr alloy by controlling the externally solidified crystals, J. Mater. Process. Technol. (2022) 117645, https://doi.org/10.1016/j.jmatprotec.2022.117645.

[93] Pavlovic-Krstic J. Impact of casting parameters and chemical composition on the solidification behaviour of Al-Si-Cu hypoeutectic alloy. Thesis 2010. Faculty of Mechanical Engineering. Magdeburgo University (Germany).
[94] R. Kralik, L. Battosova, B. Kihoulou, D. Preilser, M. Cieslar, High-temperature phase transformations in Al-Li-Cu-Mg-Zr-Sc alloy studied via in situ electron microscopy, Crystals 14 (2) (2024) 136, https://doi.org/10.3390/cryst14020136.
[95] J. Zhang, Y.N. Huang, C. Mao, P. Peng, Structural, elastic, and electronic properties of θ (Al2Cu) and S (Al2CuMg) strengthening precipitates in Al–Cu–Mg series alloys: first-principles calculations, Solid State Commun. 152 (23) (2012) 2100–2104, https://doi.org/10.1016/j.ssc.2012.09.003.
[96] K. Wen, H. Yan, L. Yan, H. Liu, W. Xiao, Y. Li, G. Gao, R. Liu, W. Ren, Evolution of S(Al2CuMg) Phase During Fabrication Process and its Influence on Mechanical Property in a Commercial Al-6.5Zn-2.4Mg-2.2Cu Alloy. In Advances in Machinery. Materials Science and Engineering Application IX, IOS Press: Amsterdam, The Netherlands, 2023, pp. 155–165.
[97] N.A. Belov, N.N. Avksenteva, Quantitative analysis of the Al –Cu –Mg – Mn – Si phase diagram as applied to commercial aluminum alloys of series 2xxx, Met. Sci. Heat. Treat. 55 (2013) 7, https://doi.org/10.1007/s11041-013-9635-3.
[98] C. Mondal, A.K. Mukhopadhyay, On the nature of T(Al2Mg3Zn3) and S (Al2CuMg) phases present in as-cast and annealed 7055 aluminum alloy, Mater. Sci. Eng.: A 391 (1-2) (2005) 367, https://doi.org/10.1016/j.msea.2004.09.013.
[99] K. Lenka, T. Eva, S. Ivana, Consequences of inappropriate temperatures of the solution heat treatment in Al-Si-Cu Cast alloy, Defect Diffus. Forum 405 (2020) 357.
[100] P. Prakash, O. Parkash, D. Kumar, Structure and mechanical behavior of in situ developed Mg2Si phase in magnesium and aluminum alloys – a review, RSC Adv. 61 (2020).
[101] X. Zhao, P. Wang, Y. Yang, S. Wang, Q. Zhao, J. Sun, Effect of artificial ageing treatment on the mechanical properties and regulation of precipitated phase particles of high-pressure die-cast thin-wall AlSi10MnMg longitudinal carrier, Material 16 (12) (2023) 4369, https://doi.org/10.3390/ma16124369.
[102] M. Warmuzek, Aluminum Silicon Casting Alloys Atlas of Microfractographs, ASM International, 2004.
[103] M. Azarbarmas, M. Emamy, J. Rassizadehghani, M. Alipour, M. Karamouz, The influence of beryllium addition on the microstructure and mechanical properties of Al–15%Mg 2 Si in-situ metal matrix composite, Mater. Sci. Eng. 528 (28) (2012) 8205, https://doi.org/10.1016/j.msea.2011.07.048.
[104] H. Mae, X. Teng, Y. Bai, T. Wierzbicki, Comparison of ductile fracture properties of aluminum castings: Sand mold vs. metal mold, Int. J. Solids Struct. 45 (1) (2008) 1430, https://doi.org/10.1016/j.ijsolstr.2007.10.016.
[105] H. Mae, X. Teng, Y. Bai, T. Wierzbicki, Calibration of ductile fracture properties of a cast aluminum alloy, Mater. Sci. Eng. A 459 (1-2) (2007) 156, https://doi.org/10.1016/j.msea.2007.01.047.
[106] B. Yang, Hongwu S. Wang, S. Chen, S. Zhang, SH. Tension-compression mechanical behavior and corresponding microstructure evolution of cast A356-T6 aluminum alloy, Mater. Sci. Eng. A 821 (1-4) (2021) 141613, https://doi.org/10.1016/j.msea.2021.141613.
[107] A. Pineau, A. Benzerga, T. Pardoen, Failure of metals I e Brittle and ductile fracture, Acta Mater. 107 (11) (2016) 424, https://doi.org/10.1016/j.actamat.2015.12.034.
[108] R. Jumaidin, E. Hamzah, M.Z. Selamat, Z.M. Zulfattah, M.H.M. Hafidzal, Effect of ageing treatment on the microstructures and hardness of Fe-Ni-Cr superalloy, Int. J. Automot. Mech. Eng. 8 (1) (2014) 2229, https://doi.org/10.15282/ijame.8.2013.30.0118.
[109] S. Sarker, S. Haque, S. Azad, M. Hasan, The effects of solution heat treatment on the microstructure and hardness of an aluminum-4% copper alloy with added nickel and tin, J. Alloy. Metall. Syst. 4 (15) (2023) 100042, https://doi.org/10.1016/j.jalmes.2023.100042.
[110] F. Czerwinski, Thermal stability of aluminum alloys, Materials 13 (15) (2020) 1441, https://doi.org/10.3390/ma13153441.
[111] B. Yang, S.F. Chen, S. Hongwu, S.H. Zhang, Effects of microstructure coarsening and casting pores on the tensile and fatigue properties of cast A356-T6 aluminum alloy: a comparative investigation), Mater. Sci. Eng. A (2022) 144106, https://doi.org/10.1016/j.msea.2022.144106.
[112] Sanchez J.M., Propiedades tribológicas y de fatiga de nuevas aleaciones de aluminio basadas en el concepto de alta entropía. Mechanical Engineering 2021, University of the Basque Country, Spain.
[113] Y.K. Kim, S. Yang, K.A. Lee, Superior temperature-dependent mechanical properties and deformation behavior of equiatomic cocrfemnni high-entropy alloy additively manufactured by selective laser melting, Sci. Rep. 10 (2020) 8045.
[114] H. Diao, X. Xie, F. Sun, K.A. Dahmen, P.K. Liaw, Mechanical properties of high-entropy alloys, Fundam. Appl. (2016) 181–236.
[115] L. Cui, Z. Zhang, X.G. Chen, Development of lightweight Al-based entropy alloys for elevated temperature applications, J. Alloy. Compd. 938 (4) (2022) 169619, https://doi.org/10.1016/j.jallcom.2022.168619.